The Canadian Mineralogist
Vol. 35, pp. 543-570 (1997)

PETROLOGY AND GEOCHEMISTRY OF PYROXENITE DYKES IN UPPER MANTLE PERIDOTITES OF THE NORTH ARM MOUNTAIN MASSIF, BAY OF ISLANDS OPHIOLITE, NEWFOUNDLAND: IMPLICATIONS FOR THE GENESIS OF BONINITIC AND RELATED MAGMAS[1]

VERONIKA VARFALVY[2] AND RÉJEAN HÉBERT

Département de Géologie et de Génie Géologique, Université Laval, Sainte-Foy, Québec G1K 7P4

JEAN H. BÉDARD

Commission Géologique du Canada, Centre Géoscientifique de Québec, Case Postale 7500, Sainte-Foy, Québec G1V 4C7

MARC R. LAFLÈCHE

INRS-Géoressources, Centre Géoscientifique de Québec, Case Postale 7500, Sainte-Foy, Québec G1V 4C7

ABSTRACT

Upper-mantle rocks form the basal part of the North Arm Mountain ophiolitic massif (NAMM), in Newfoundland. They are dominantly composed of plastically deformed refractory harzburgite, and are cut by numerous dykes of pyroxenite. These dykes range from orthopyroxenite to websterite and clinopyroxenite, and contain variable amounts of olivine, spinel and disseminated Fe–Ni sulfides. Whole-rock and mineral chemistries of the pyroxenitic dykes are characterized by low contents of Al, Na, K, Ta, Zr, Hf, Ti and the *REE*, high Mg-numbers, high Cr and Ni contents, and *LILE* enrichment relative to less incompatible elements. Magmas calculated to have coexisted with the pyroxenites have strongly depleted *HREE*, Ta, Zr, Hf and Ti contents, with *LILE* enrichment relative to MORB. The mineral and geochemical data suggest that the pyroxenites have not directly crystallized from primary magmas generated by the melting of ultra-depleted mantle; rather, the relevant magmas acquired the signatures of such mantle by reacting and reaching equilibrium with large volumes of variously depleted peridotites at shallower levels during their migration through the mantle. We propose that the variety of compositions among melts related to the pyroxenites resulted from fractional crystallization of olivine ± spinel, assimilation of clinopyroxene from the wallrocks, and magma mixing, in various proportions, involving a primary low-Ti magnesian tholeiitic component and low fractions ($\leq$10%) of melts produced by partial remelting of surrounding metasomatized harzburgites or lherzolites. The composition of NAMM intra-mantle pyroxenite dykes resembles that of modern magnesian andesites, including boninites found in the western Pacific, which suggests that the NAMM mantle have been affected by intraoceanic fore-arc magmatism. If the analogy holds true, primitive boninite melts may have undergone similar interactions with depleted mantle, and acquired their unusual signature by reacting with large volumes of variously depleted peridotites during their migration through the mantle.

Keywords: pyroxenite, peridotite, boninite, ophiolite, petrology, geochemistry, upper mantle, magma–mantle interactions, subduction, arc magmatism, North Arm Mountain massif, Bay of Islands, Newfoundland.

SOMMAIRE

La partie inférieure du massif ophiolitique de North Arm Mountain (NAMM), à Terre-Neuve, est formée de roches du manteau supérieur. Ces roches se composent principalement de harzburgites réfractaires, plastiquement déformées, et recoupées de nombreux dykes de pyroxénite. Ces dykes varient en composition, de orthopyroxénite, webstérite à clinopyroxénite, et contiennent des quantités variables d'olivine, de spinelle et de sulfures de Fe–Ni disséminés. La composition chimique (roche totale et chimie minérale) des dykes pyroxénitiques de NAMM indique de faibles teneurs en Al, Na, K, Ta, Zr, Hf, Ti et terres rares, de valeurs de Mg# élevées, des teneurs élevées en Cr et Ni, ainsi qu'un enrichissement relatif en éléments lithophiles à large rayon comparativement aux éléments moins incompatibles. Les compositions calculées des magmas qui auraient coexisté avec les pyroxénites présentent des teneurs extrêmement appauvries en terres rares lourdes, Ta, Zr, Hf et Ti, avec un enrichissement relatif en éléments lithophiles à large rayon par rapport aux basaltes des crêtes médio-océaniques. Les pyroxénites

---

[1] Geological Survey of Canada contribution number 1997036

[2] *E-mail address*: varfalvy@ggl.ulaval.ca

de NAMM n'auraient pas directement cristallisé à partir de magmas primaires, générés par la fusion d'un manteau ultra-appauvri. Plutôt, les magmas qui leur sont reliés auraient acquis la signature d'un tel manteau par réaction et ré-équilibrage avec de larges volumes de péridotites appauvries de façon variable, à de faibles profondeurs, durant leur migration à travers le manteau. Nous proposons que la variété, en composition, de ces magmas reliés aux pyroxénites de NAMM résulte de la cristallisation fractionnée d'olivine ± spinelle, de l'assimilation de clinopyroxène dissous à partir des épontes, et de mélange de magmas, en proportions variées, impliquant un composant tholéiitique primaire, riche en Mg et pauvre en Ti, et de faibles fractions (≤10%) de liquides produits par la refusion des harzburgites et des lherzolites métasomatisées environnantes. La composition des dykes de pyroxénite du manteau de la suite NAMM ressemble à celles des andésites modernes riches en Mg, dont les boninites, ce qui suggère que la portion du manteau du NAMM a été affectée par un magmatisme intra-océanique d'avant-arc. Si l'analogie se révèle correcte, les magmas boninitiques primitifs auraient subi des interactions semblables avec le manteau appauvri, et auraient acquis leur signature particulière en réagissant avec de larges volumes de péridotites appauvries durant leur migration à travers le manteau.

Mots-clés: pyroxénite, péridotite, boninite, ophiolite, pétrologie, géochimie, manteau supérieur, interactions magma–manteau, subduction, magmatisme d'arc, massif de North Arm Mountain, Bay of Islands, Terre-Neuve.

INTRODUCTION

Pyroxenite veins are a characteristic feature of most upper-mantle peridotites in ophiolites. They usually are coarse-grained, range from a few cm to 1 m in thickness, and range in composition from orthopyroxenite to websterite and clinopyroxenite, with minor spinel as a common accessory phase, but some examples may also contain olivine, garnet, primary amphibole, plagioclase and sulfides. Several authors have concluded that these pyroxenite veins represent conduits along which melts migrated within the upper mantle (*e.g.*, Podvin *et al.* 1985, Frey *et al.* 1985, Reuber *et al.* 1985, Wilshire 1987, Suen & Frey 1987, Bodinier *et al.* 1987, 1990, Kelemen 1990, Takahashi 1992, Edwards 1995, Garrido & Van der Wal 1995, Varfalvy *et al.* 1996). Several studies on the petrology and geochemistry of intra-mantle pyroxenite dykes and their host peridotites have revealed a complex magmatic history of multiple intrusive events, involving distinct melts derived by multi-stage crystal–melt segregation from different sources (Suen & Frey 1987, Bodinier *et al.* 1987, Edwards 1991, 1995, Garrido 1995, Garrido & Van der Wal 1995). However, pyroxenite dykes are commonly affected by intense plastic deformation, making it difficult to establish a relative chronology of intrusion and deformation events. Moreover, assimilation-reaction processes between the intrusive melts and host peridotites may change the primary composition of intrusive melts and host peridotites, complicating the interpretation of the geochemical signature and the origin of these melts (Quick 1981, Podvin *et al.* 1985, Kelemen & Ghiorso 1986, Kelemen 1990, Varfalvy *et al.* 1996). In this paper, we present new whole-rock trace-element data from the mantle rocks of the North Arm Mountain massif, in the Bay of Islands ophiolite, Newfoundland, in order to better define the nature of the melts from which mantle-hosted pyroxenite dykes formed, and the types of processes that drove the chemical evolution of these melts.

GEOLOGICAL SETTING

The Bay of Islands ophiolitic complex (BIOC) represents a klippe of the Appalachian Dunnage Zone (Williams 1979) that was emplaced onto the collapsed, passive continental margin of eastern North America during the Early to Middle Ordovician Taconian Orogeny (Williams & Stevens 1974, Cawood *et al.* 1988, Cawood & Suhr 1992). It is formed of four distinct ophiolitic massifs; from north to south, these are (Fig. 1) Table Mountain, North Arm Mountain, Blow-Me-Down Mountain and Lewis Hills (Williams & Malpas 1972, Irvine & Findlay 1972). The BIOC is tectonically juxtaposed to the west (Fig. 1) against a complex assemblage of metamorphosed and deformed ophiolitic rocks referred to as the Coastal Complex (CC) (Williams 1973). U/Pb ages obtained on zircon from both complexes indicate that the CC (505 + 3 /–2 Ma) is significantly older than the BIOC (484 ± 5 Ma) (Jenner *et al.* 1991). A high-temperature metamorphic sole to the BIOC is present, generally less that 200 m thick, along the eastern margin of all four massifs (Williams 1973, Williams & Smyth 1973), and is interpreted to represent the high-temperature shear zone along which the ophiolite slab was detached (Williams & Smyth 1973, Jamieson 1986, Cawood & Suhr 1992). Ar/Ar and K–Ar results obtained on amphibolites in the metamorphic sole of the North Arm Mountain massif give cooling ages of around 470 Ma (Dallmeyer & Williams 1975, Archibald & Farrar 1976), which provides a minimum age for the development of the detachment-related high-strain mylonitic fabrics of the BIOC metamorphic sole, and constrains the interval between generation and obduction of the BIOC at around 10 Ma (Cawood & Suhr 1992).

The North Arm Mountain massif (NAMM) of the BIOC (Fig. 1) preserves a complete ophiolitic sequence that consists, from base to top, of (1) upper mantle tectonites, (2) lower-crust interlayered ultramafic and mafic cumulates and intrusions, (3) layered and foliated

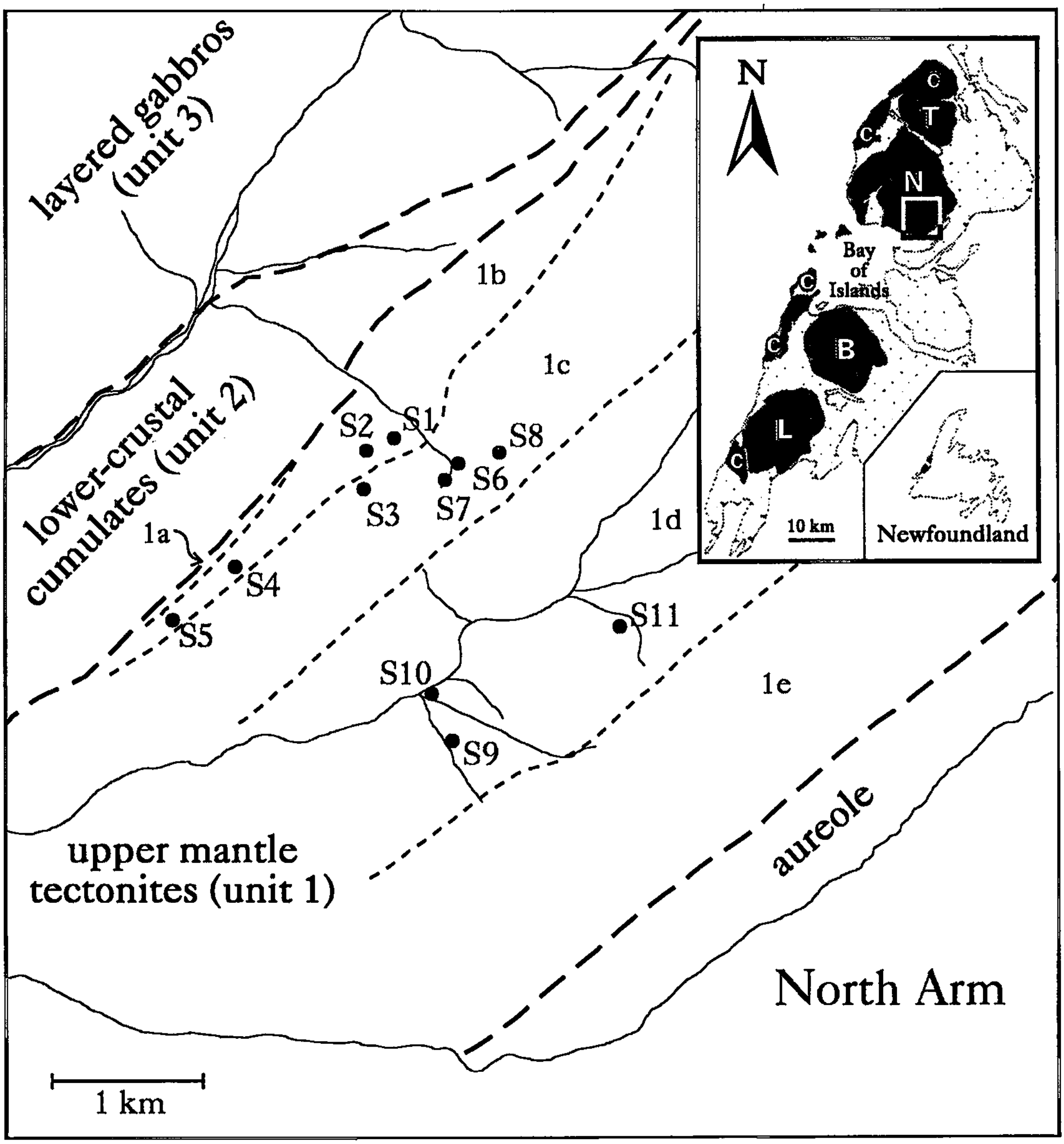

FIG. 1. Map of part of the North Arm Mountain massif of the Bay of Islands Ophiolite and sample locations (•): basal metamorphic aureole (aureole), upper-mantle tectonites (units 1a to 1e), transitional lower-crust unit made of interlayered ultramafic and mafic cumulates (unit 2), layered adcumulate gabbros (unit 3). Inset, ophiolite massifs of the Bay of Islands ophiolite complex: Table Mountain (T), North Arm Mountain (N), Blow Me Down Mountain (B), Lewis Hills (L), and terranes forming the Coastal Complex (C), redrawn from Edwards (1990).

adcumulate crustal gabbros, (4) porphyritic gabbros, hornblendites and plagiogranites, (5) sheeted dykes, (6) lavas and sediments (Riccio 1976, Malpas 1976, Casey *et al.* 1981, Bédard 1991). Upper mantle rocks underlie an area of 60 km^2, with an apparent thickness of 4–5 km between the basal metamorphic sole and the overlying crust. NAMM mantle rocks commonly consist of plastically deformed harzburgites that are interbanded on a cm scale with lherzolites near the contact with the overlying crust, and that grade down to coarse-grained lherzolites near the basal metamorphic aureole (Smith 1958, Malpas 1976, Suen *et al.* 1979, Varfalvy 1994, Varfalvy *et al.* 1995, 1996). Bands of subconcordant to discordant dunite (less than 1 m thick) with diffuse contacts are common. NAMM mantle peridotites are cut by numerous pyroxenite intrusions, which are the subject of this paper.

The mantle section is subdivided into five structural and petrological units (from top to bottom: 1a to 1e) that trend N40°, parallel to the crust–mantle interface (Fig. 1) (Berclaz *et al.* 1994, Varfalvy *et al.* 1996). Unit 1a immediately underlies the crust. It consists of massive, fine-grained mylonitic to ultramylonitic harzburgite to lherzolite. Unit 1a structures are perfectly coaxial with those of the lowermost crust. Unit 1a thins and becomes discontinuous toward the southwestern part of the massif. The underlying unit 1b is principally composed of lherzolite and harzburgite, with subordinate plagioclase wehrlite. Steeply dipping, cm-scale layering is well developed. Bedding and mineral foliations are parallel to those of unit 1a. Individual layers show significant variations in their pyroxene:olivine and orthopyroxene:clinopyroxene ratios. There are numerous dunitic, orthopyroxenitic, websteritic, clinopyroxenitic, wehrlitic and gabbroic minor intrusions (dykes, sills and veinlets), variably transposed and boudinaged by plastic deformation. The immediately underlying unit 1c is distinguished from unit 1b by the abundance of dunite dykes, layers and pods, and the absence of plagioclase wehrlite, gabbroic and clinopyroxenitic intrusions. The underlying unit, 1d, is dominated by harzburgite, but contains numerous concordant to subconcordant orthopyroxenite intrusions. Isoclinal fold closures are common. Planar fabrics are weaker than in unit 1c, with less abrupt dips. A fifth unit, unit 1e, directly overlies the metamorphic sole. It is composed of harzburgite that grades downward in the section to coarse-grained lherzolite. Numerous clinopyroxene-bearing mylonitic to ultramylonitic shear zones parallel the principal fabric seen in the metamorphic sole (Berclaz *et al.* 1994, Hébert *et al.* 1996).

PETROLOGICAL DESCRIPTIONS OF THE PYROXENITE DYKES

Concordant to subconcordant orthopyroxenite intrusions are observed throughout the mantle section. Clinopyroxenite and websterite intrusions (including some composite veins with a clinopyroxenitic core and an orthopyroxenitic margin) mainly occur in the vicinity of the crust–mantle interface. They are particularly common in unit 1a, in the northeastern part of the massif. Here they are thin, transposed into the foliation, and boudinaged. They are also fairly common in unit 1b, in the southwestern part of the massif. Here they are transposed into the foliation to varying degrees, and are locally folded and boudinaged. Rare intrusions of websterite are also observed in unit 1c, and some thin and deformed olivine-bearing clinopyroxenite veins also occur in unit 1e. Concordant gabbroic veinlets were only observed in unit 1b. The following pyroxenitic intrusions were sampled and studied; eight consist of orthopyroxenite (S3–O, S5–O, S6–O, S7–O, S8–O, S9–O, S10–O, S11–O), three consist of clinopyroxenite (S1–C1, S1–C2, S2–C), one is websterite (S4–W), and three are websteritic composite veins (S1–CV1, S1–CV2, S5–CV). The prefixes S1 to S12 in sample names refer to sites 1 to 12 plotted on Figure 1. Based on their composition (the mineral and whole-rock compositions will be discussed in detail later), the pyroxenite intrusions were subdivided in four distinct suites: suite I comprises orthopyroxenites S3–O, S6–O, S7–O, S8–O and S9–O, suite II comprises orthopyroxenites S5–O, S10–O, S11–O and composite vein S5–CV, suite III consists of websterite S4–W and composite vein S1–CV2, and suite IV comprises clinopyroxenites S1–C1, S1–C2 and composite vein S1–CV1. These pyroxenite intrusions range in thickness from 5 to 15 cm (clinopyroxenite and websteritic dykes) and from 10 to 30 cm (orthopyroxenite dykes). The relative chronology among the pyroxenite intrusions has not been established with precision. They comprise less than 5% of the total volume of NAMM mantle rocks, and different types rarely occur together.

Pyroxenitic dykes contain variable amounts of olivine (<10% modal), except for S3–O and S7–O orthopyroxenites, which are olivine-free, and contain 1–2% modal spinel (Varfalvy 1994). Rare, fine-grained (<0.1 mm), disseminated Fe–Ni-sulfide grains (pyrrhotite and pentlandite) are observed only in clinopyroxene-rich intrusions. Most of the pyroxenitic intrusions are zoned, from more olivine-rich margins to a pyroxene-rich core. Clinopyroxenite and websteritic intrusions are zoned from more orthopyroxene-rich margins to a more clinopyroxene-rich core. This zonation is gradual in clinopyroxenites and S4–W websterite, but in composite veins, a sharp contact separates the orthopyroxenite margin from the clinopyroxenite core. In thin section, pyroxenites typically exhibit a medium- to coarse-grained (0.1–10 mm) polygonal granular texture, with 120° triple junctions between pyroxene grains. Pyroxene grains rarely have exsolution lamellae, but commonly show microtextures such as kink-bands and shear-bands with recrystallized subgrain boundaries, indicative of plastic deformation. Olivine grains are interstitial to pyroxene, with irregular contacts, and, where more abundant, form chains of small grains (<1 mm) distributed along pyroxene grain-boundaries. Orthopyroxenites usually contain less that 2% modal clinopyroxene, except for S3–O orthopyroxenite, which contains 4% modal clinopyroxene. Clinopyroxenites may contain 1–7% modal orthopyroxene. In orthopyroxenites, rare clinopyroxene is finer grained (<1 mm) and interstitial, whereas in clinopyroxenites, it is the orthopyroxene that is finer-grained (<3 mm) and interstitial. Interstitial fine-grained clinopyroxene in orthopyroxenites probably represents recrystallized exsolutions (Varfalvy *et al.* 1996). Accessory spinel occurs as red-brown, dark brown or opaque euhedral grains disseminated throughout the intrusions, and as rounded grains associated with olivine. Spinel grains are coarser (<0.8 mm) in orthopyroxenites, and finer-grained (0.1–0.2 mm) in clinopyroxene-rich intrusions. Primary igneous amphibole occurs as interstitial pale brown hastingsite to pargasite (<1% modal) in one intrusive body of orthopyroxenite from the vicinity of the crust–mantle interface, but was not found (or not preserved) in any of the other pyroxenite dykes. Retrograde amphiboles (assemblage anthophyllite – cummingtonite – tremolite) after pyroxenes, and serpentine (<2% modal) after olivine, are observed locally. The common presence of retrograde amphiboles (tremolite, anthophyllite) indicates partial re-equilibration during an episode of circulation of hydrous fluid at a temperature below 700°C (Jenkins 1983). Since these fluids can be expected to circulate along the same fractures and grain boundaries as where primary amphiboles are found, the lack of primary amphiboles may reflect preferential alteration along such sites (Varfalvy *et al.* 1996).

Wallrock harzburgites that are in direct contact (≤2 cm wide) with pyroxenite dykes have systematically lower modal clinopyroxene, and may be slightly enriched in modal orthopyroxene, in comparison with more distal peridotite hosts (>1 m from the margins of the dykes) (Varfalvy *et al.* 1996). This clinopyroxene-depleted contact zone seems to extend more than 2 cm from an intrusion's margins into the wallrocks. A well-developed porphyroclastic to mylonitic texture commonly occurs at the contact between wallrock harzburgite and intrusive orthopyroxenite. The harzburgite–pyroxenite transitions are generally sharp, and marked by a thin (5 mm wide) microgranoblastic olivine – orthopyroxene – spinel rim that is plated along the margin of the pyroxenite, and that locally breaks up and lenses out into the mylonitized wallrock. However, some intrusive pyroxenites have gradual contacts (clinopyroxenite S1–C1 and orthopyroxenite S10–O). The contact zone is about 5 mm wide, and is characterized by an inward decrease in the proportion and grain size of pyroxene, and an increasingly interstitial (to olivine) habit of pyroxene. The existence of mylonitic wallrocks and the abundance of textures diagnostic of plastic deformation in the pyroxenite dykes suggest that the intrusions were injected into and crystallized within zones of active high-temperature deformation, which may have guided emplacement of the intrusions.

ANALYTICAL METHODS

Electron-microprobe analyses of olivine, orthopyroxene, clinopyroxene, spinel and some accessory amphibole and sulfides were carried out at Université Laval with an ARL electron microprobe operated at 20 kV and 0.1 mA. Beam diameter was 3 μm; natural standards were used. Integration time was 10 seconds for each measurement, which was repeated three times. The data were corrected using a ZAF program (Bence & Albee 1968). Replicated analyses of standards indicate that the determinations have a relative accuracy of 1 to 2% for major elements. Representative results of mineral analyses are reported in Tables 1 to 4.

Whole-rock chemical analyses were undertaken on 14 NAMM pyroxenite dykes. For composite dykes S1–CV1 and S1–CV2, analyzed powdered samples included orthopyroxenitic margins and clinopyroxenitic cores, whereas for composite dyke S5–CV, only orthopyroxenitic margins were analyzed. The analyses were done by inductively coupled plasma – atomic emission spectrometry (ICP–AES) at the Laboratoire de Plasma, INRS-Géoressources, Complexe Géoscientifique de Québec. Concentrations of major elements and the trace elements Sc, V, Cr, Ni, Zn and Cu were obtained from solutions prepared from powdered sample rocks. Precision and accuracy are generally better than 1% in cases where the concentrations of an element are well above its detection limits. Detection limits range between 0.001 and 0.005 wt.% for major elements (expressed as oxides). Detection limits are ~4 ppm for Cr, Ni and V, and ~1 ppm for Sc, Cu and Zn. Loss on ignition (LOI) is included in the totals reported below in Table 5.

Whole-rock Rb, Sr, Zr, Nb, Cs, Ba, Hf, Ta, Th, U and rare-earth-element (*REE*) concentrations were determined using inductively coupled plasma – mass spectrometry (ICP–MS) at the Laboratoire de Plasma, INRS-Géoressources, following successive acid digestions of powdered rock samples, according to a procedure developed at the Complexe Géoscientifique de Québec by M.R. Laflèche. Integration time was 60 seconds for each measurement, which was repeated three times. The natural standard UB–N was used for control. Teflon beakers and doubly-distilled reagents were used, and precautions were taken during sample preparation and dissolution to avoid contamination. Replicate analyses of standards and samples indicate that results are accurate to 2–8% (depending on the element). Detection limits range between 0.001 and 0.01 × chondrite; element concentrations in C1 chondrite are from Sun & McDonough (1989). Results of whole-rock trace-element analyses performed by ICP–AES and ICP–MS are presented in Table 6.

MINERAL CHEMISTRY

In terms of spinel, orthopyroxene and olivine compositions, the pyroxenite intrusions show a wide compositional range that contrasts with their peridotite hosts, which have narrower compositional ranges (Figs. 2, 3 and 4). The compositional range seen in minerals of the host peridotites is characteristic of extremely residual ophiolitic mantle (Dick 1977, 1989, Hamlyn & Bonatti 1980, Dick & Fisher 1984, Michael & Bonatti 1985, Smith & Elthon 1988).

Spinel grains in pyroxenitic intrusions show large variations in their Cr/Al and Mg/Fe values (Table 1). The Ti content of spinel (<0.1 wt.% TiO_2) from all

TABLE 1. REPRESENTATIVE COMPOSITIONS OF SPINEL

Sample	S2-C	S5-O	S5-CV	S6-O
Type[1]	cpxite	opxite II	comp	opxite I
TiO_2 (wt.%)	0.04	0.02	0.05	0.12
Al_2O_3	45.03	35.94	17.52	14.37
FeO	15.89	14.84	18.69	22.09
$Fe_2O_3^{+}$	2.52	0.66	1.63	2.91
MgO	15.14	14.87	10.77	8.47
Cr_2O_3	19.97	32.86	51.11	51.95
MnO	0.21	0.11	0.09	0.12
Total	99.32	99.30	99.86	100.03
Cr/Cr+Al	0.229	0.380	0.662	0.708
Fe^{2+}/Fe^{2+}+Mg	0.371	0.359	0.493	0.594

[1] Notes: cpxite, clinopyroxenite; webs, websterite; comp, composite vein; opxite I, Type I orthopyroxenite; opxite II, Type II orthopyroxenite. $^{+}$ recalculated from stochiometry.

pyroxenite dykes is low and near detection limits. On the basis of Cr/Al and Mg/Fe values of the spinel, orthopyroxenite dykes can be divided into two subtypes (Fig. 2): type-I orthopyroxenites S3–O, S6–O, S7–O, S8–O and S9–O form a first group; these samples contain Cr-rich spinel comparable in composition to that observed in boninites. Type-II orthopyroxenites S5–O and S10–O form a second group, in which the spinel has higher Al and Mg contents, which are comparable to those in spinel from backarc-basin basalts. Spinel grains in type-III websterite S4–W are significantly richer in iron and plot apart from both groups. Type-IV clinopyroxenites S1–C1 and S2–C contain high-Al Mg-rich spinel. In terms of their spinel chemistry, composite veins S1–CV1 (type-IV suite) and S5–CV (type-II suite) plot between their respective suite and type-I orthopyroxenite suite. Spinel compositions from type-IV clinopyroxenites to type-II orthopyroxenites and to type-I orthopyroxenites S9–O and S8–O form a general trend of marked Cr-enrichment coupled with slight Fe-enrichment similar to the trend shown for spinel compositions during increasing partial melting of mantle peridotite (Dick & Bullen 1984). However, spinel in type-IV pyroxenites has, on

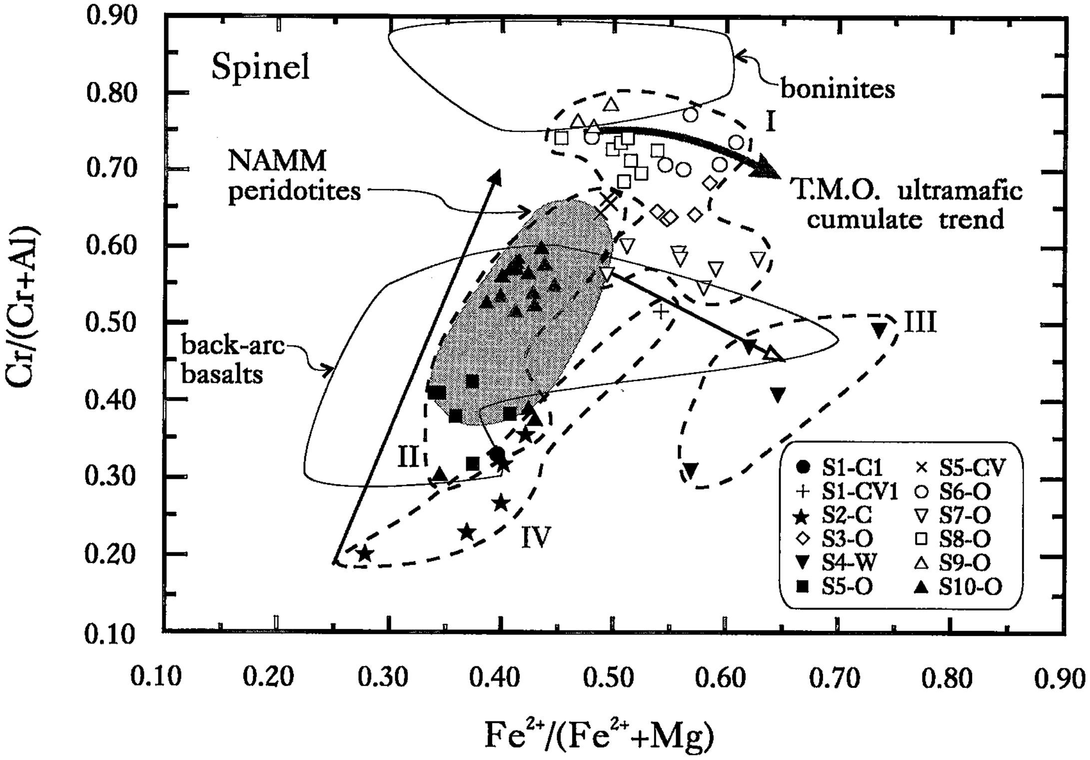

FIG. 2. [Cr/(Cr + Al)] *versus* [$Fe^{2+}/(Fe^{2+}$ + Mg)] of spinel from pyroxenite dykes. Dashed fields enclose suites of type-I, type-II, type-III and type-IV pyroxenite dykes. Also shown are data for spinel from NAMM mantle peridotites (grey field), after Varfalvy *et al.* (1996), boninites after Dick & Bullen (1984), and backarc basalts after Dick & Bullen (1984) and Hawkins & Melchior (1985). Arrows indicate trends shown for spinel compositions during partial melting of mantle peridotite (black arrow) and for fractional crystallization of olivine (white arrow), after Dick & Bullen (1984). The heavy black arrow represents the fractionation trend observed for spinel in the lower crust ultramafic cumulates of the Appalachian Thetford Mines ophiolite (T.M.O.; Laurent & Kacira 1987).

average, a slightly higher Fe content than that in type-II orthopyroxenites, which could be attributed to olivine fractionation. On the other hand, spinel in type-I orthopyroxenites, from S9–O to S8–O and to S6–O, form a trend of marked Fe-enrichment coupled with slight Cr-depletion. Variations of spinel compositions within a given sample, for all type-I orthopyroxenites, also define this Fe–Al-enrichment trend. This trend is similar to the trend observed for chromian spinel in the lower-crust ultramafic cumulates of the Appalachian Thetford Mines ophiolite (Laurent & Kacira 1987) and is consistent with a trend imposed by the fractional crystallization of olivine. Spinel compositions in type-III websterite S4–W, richer in Fe and Al, fall on the extension of the trend formed by type-I orthopyroxenites, and so could

TABLE 2. REPRESENTATIVE COMPOSITIONS OF ORTHOPYROXENE

Sample Type[1]	S1-C1 cpxite	S5-O opxite II	S5-CV comp	S8-O opxite I
SiO_2 (wt.%)	55.49	55.95	56.90	57.20
TiO_2	0.02	0.00	0.00	0.00
Al_2O_3	2.47	2.63	1.17	0.88
FeO	6.35	6.00	6.01	5.79
MgO	33.26	33.64	34.13	34.49
CaO	0.92	0.92	1.02	1.01
Na_2O	0.09	0.12	0.11	0.11
Cr_2O_3	0.35	0.44	0.36	0.30
MnO	0.14	0.17	0.22	0.14
Total	99.09	99.87	99.92	99.92
En	88.73	89.31	89.26	89.67
Fs	9.50	8.94	8.82	8.45
Wo	1.76	1.76	1.92	1.89
$Mg/Mg+Fe^{2+}$	0.903	0.909	0.910	0.914

[1] see notes in Table 1.

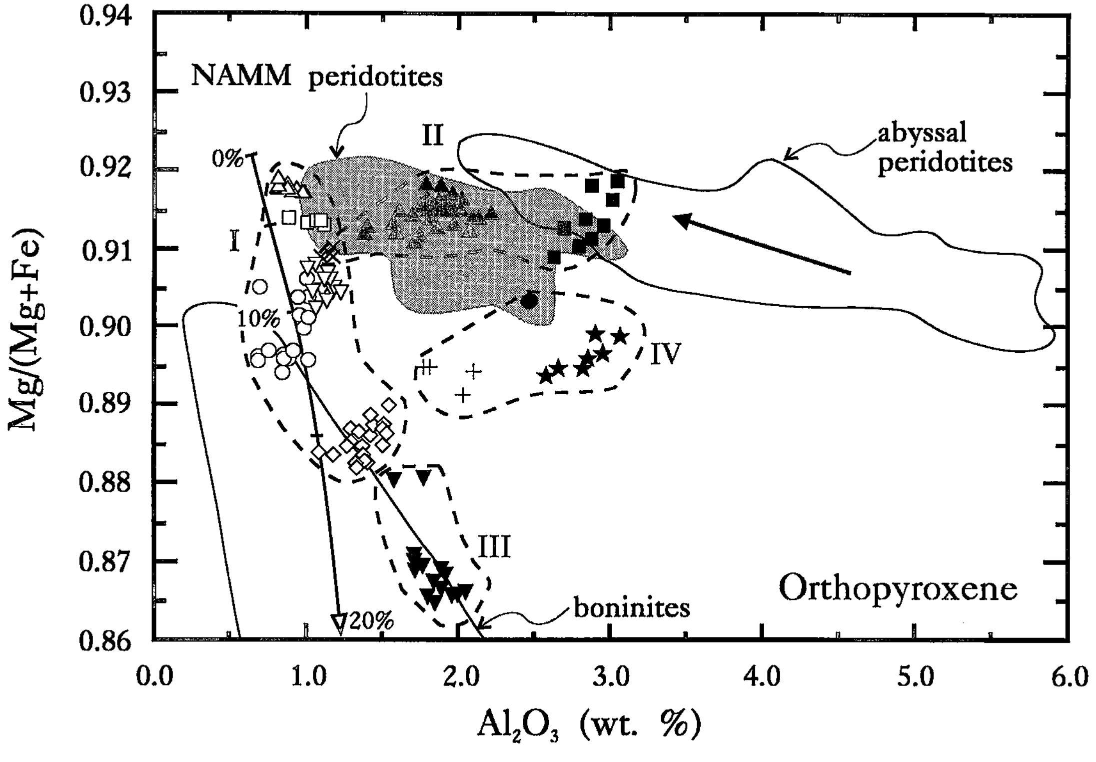

FIG. 3. [Mg/(Mg + Fe)] *versus* Al_2O_3 wt.% of orthopyroxene from pyroxenite dykes. Dashed fields enclose suites of type-I, type-II, type-III and type-IV pyroxenite dykes. Also shown are data fields for orthopyroxene from NAMM mantle peridotites (grey field), after Varfalvy *et al.* (1996), and from abyssal peridotites, after Dick & Fisher (1984). The black arrow in the abyssal peridotite field indicates the trend shown for orthopyroxene compositions during partial melting of mantle peridotite, after Smith & Elthon (1988). The boninite field is drawn from orthopyroxene phenocrysts in boninites from Bonin Islands (Taylor *et al.* 1994), Troodos (Cameron 1985), New Caledonia (Cameron 1989), Izu–Bonin fore-arc (Van der Lann *et al.* 1992), Mariana trench (Bloomer & Hawkins 1987), and the northern termination of the Tonga trench (Falloon *et al.* 1989, Sobolev & Danyushevsky 1994). The scaled white arrow is a calculated olivine-fractionation curve, from 0 to 20% of crystallization, assuming that no Al enters the fractionating olivine. The orthopyroxene/liquid Fe–Mg exchange-reaction coefficient used was 0.27 (Kinzler & Grove 1992). The orthopyroxene/liquid partition coefficient for Al was assumed to be 0.06. This value represents a calculated mean concentration of Al in orthopyroxene phenocryst over Al in glass or groundmass in boninites from the Tonga trench (Falloon *et al.* 1989). Symbols are the same as in Figure 2.

be related to them by a fractional crystallization relationship.

The orthopyroxene in pyroxenitic intrusions is enstatite-rich (En_{91-85}, Table 2), and its Ca content is very low (average <1.0 wt.% CaO). Its TiO_2 and NaO_2 contents are respectively <0.05 and <0.1 wt.%. Al and Fe contents correlate with those of their associated spinel. Type-I orthopyroxenites have Al-poor orthopyroxene similar to orthopyroxene phenocrysts found in boninites, whereas orthopyroxene in type-II orthopyroxenites and type-IV clinopyroxenites are richer in Al (Fig. 3). Here again, composite veins (type-IV S1–CV1 and type-II S5–CV) plot between their respective suite and type-I orthopyroxenite suite. Orthopyroxene compositions, from type-IV clinopyroxenites to type-II orthopyroxenites and to type-I orthopyroxenites S9–O and S8–O, form a general trend of Fe–Al-depletion roughly compatible with increasing partial melting of mantle peridotite (Smith & Elthon 1988). However, orthopyroxene in type-IV clinopyroxenites show higher Fe-contents, which could be attributed to olivine fractionation. As well, the continuous trend of marked Fe enrichment and less marked Al enrichment among the orthopyroxene compositions of type-I orthopyroxenites, which is similar to the boninite trend, is consistent with a trend imposed by fractional crystallization of olivine. Orthopyroxene compositions in type-III websterite S4–W are richer in Fe and Al, falling on the extension of the type-I trend, and so could be related by a fractional crystallization relationship to type-I orthopyroxenites. It is noteworthy that for type-I and type-III suites, clinopyroxene becomes an important modal phase only in the intrusions with aluminous and iron-rich pyroxenes (type-I orthopyroxenite S3–O and type-III websterite S4–W). If this trend is caused by fractionation, then the clinopyroxene-bearing intrusions crystallized from its most evolved members.

The clinopyroxene in the pyroxenitic intrusions is nearly pure diopside ($En_{>47}Wo_{>44}$, Table 3). Its TiO_2 and NaO_2 contents are respectively <0.1 and <0.3 wt.%. Its Al and Fe contents correlate with those of their associated orthopyroxene and spinel. The Al contents of clinopyroxene in type-I orthopyroxenites and type-III websterite S4–W, respectively, range between 0.7 and 1.9 wt.% Al_2O_3 [with Mg# in the range 0.90–0.94; Mg# = 100 Mg/(Mg + Fe^{2+}), with total iron expressed as Fe^{2+}], and between 1.2 and 2.2 wt.% Al_2O_3 (with Mg# in the range 0.88–0.92). These Al contents are comparable to those of clinopyroxene phenocrysts in boninites from the northern termination of the Tonga trench (0.9–1.8 wt.% Al_2O_3, with Mg# in the range 0.86–0.91; Falloon *et al.* 1989, Sobolev & Danyushevsky 1994), but are distinct from other western Pacific boninites, which have less magnesian pyroxene phenocrysts (Falloon *et al.* 1989). The Al content of clinopyroxene in type-II orthopyroxenites and type-IV pyroxenites, respectively, range between 1.4 and 2.8 wt.% Al_2O_3 (with Mg# in the range 0.93–0.94) and between 1.8 and 3.6 wt.% Al_2O_3 (with Mg# in the range 0.91–0.93). These Al contents are comparable to those of Al-poor clinopyroxene phenocrysts in arc tholeiites from Manam island (1.2–2.6 wt.% Al_2O_3, Mg# in the range 0.84–0.89; Johnson *et al.* 1985), in backarc tholeiites from the Lau basin (2.2–4.8 wt.% Al_2O_3, Mg# in the range 0.82–0.90; Hawkins & Melchior 1985) and in boninites from the upper lava sequence of the Troodos ophiolite (1.3–4.9 wt.% Al_2O_3, Mg# in the range 0.75–0.91; Bednarz & Schmincke 1994). Clinopyroxene compositions from the type-II orthopyroxenites and type-IV pyroxenites have, however, much higher Mg-numbers than the Manam, Lau or Troodos occurrences listed.

The Mg/Fe value of olivine in the pyroxenite intrusions correlates with that of their associated pyroxenes (Table 4, Fig. 4). However, the Ni content of olivine in type-II pyroxenites (0.35–0.55 wt.% NiO) is unexpectedly higher than in Al-poor type-I orthopyroxenites (typically <0.40 wt.% NiO), which is inconsistent with increasing partial melting of peridotite from type-II pyroxenites to type-I orthopyroxenites. Olivine in type-IV

TABLE 3. REPRESENTATIVE COMPOSITIONS OF CLINOPYROXENE

Sample	S1-C1	S3-O	S4-W	S10-O
Type[1]	cpxite	opxite I	webs	opxite II
SiO_2 (wt.%)	52.35	53.69	53.58	53.37
TiO_2	0.11	0.04	0.04	0.02
Al_2O_3	3.37	1.43	2.07	2.36
FeO	2.80	2.65	3.39	2.00
MgO	17.25	17.55	17.77	17.58
CaO	23.00	23.55	22.40	24.00
Na_2O	0.30	0.23	0.10	0.09
Cr_2O_3	0.66	0.68	0.53	0.87
MnO	0.10	0.08	0.09	0.09
Total	99.94	99.95	99.99	100.42
En	48.79	48.79	49.67	48.90
Fs	4.44	4.13	5.31	3.12
Wo	46.76	47.07	45.02	47.98
$Mg/Mg+Fe^{2+}$	0.917	0.922	0.903	0.940

[1] see notes in Table 1.

TABLE 4. REPRESENTATIVE COMPOSITIONS OF OLIVINE

Sample	S2-C	S5-CV	S8-O	S10-O
Type[1]	cpxite	comp	opxite I	opxite II
SiO_2 (wt.%)	40.56	40.75	40.67	40.51
FeO	10.14	9.25	8.75	8.90
MgO	48.49	49.12	49.66	49.74
MnO	0.18	0.18	0.16	0.14
NiO	0.44	0.57	0.25	0.46
Total	99.81	99.87	99.49	99.75
Fo	89.34	90.27	90.85	90.75
$Mg/Mg+Fe^{2+}$	0.895	0.904	0.910	0.909

[1] see notes in Table 1.

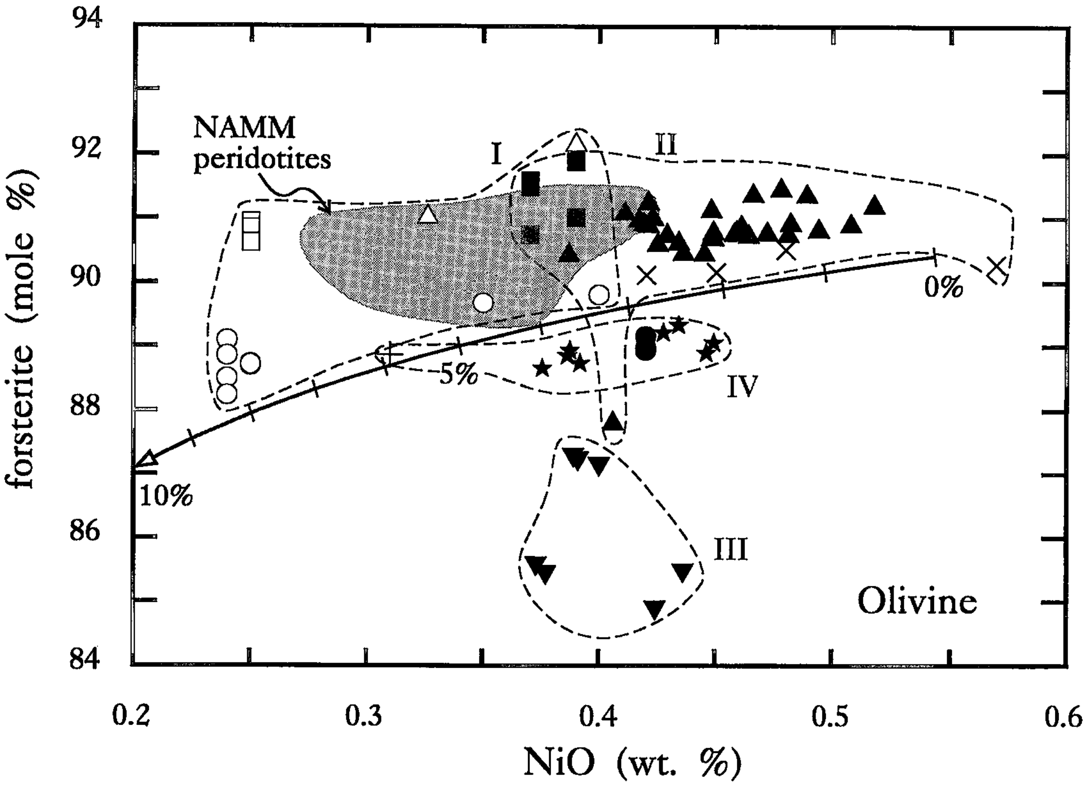

FIG. 4. Forsterite content *versus* NiO wt.% of olivine from pyroxenite dykes. Dashed fields enclose suites of type-I, type-II, type-III and type-IV pyroxenite dykes. Also shown are the data for olivine from NAMM mantle peridotites (grey field), after Varfalvy *et al.* (1996). The scaled arrow is a calculated olivine fractionation curve, from 0 to 10% of crystallization. The olivine/liquid Fe–Mg exchange-reaction coefficient used was 0.30 (Roeder & Emslie 1970). The olivine/liquid partition coefficient for Ni was calculated using the following equation (for $Fo_{ol} > 0.65$) [$^{ol/liq}D_{Ni} = -0.8480769 \times (100 \times Fo_{ol}) + 87.37307692$] from Budahn (1986). The $^{ol}D_{Ni}$ varied from 10.7 to 13.5, for 0 to 10% of crystallization. Symbols are the same as in Figure 2.

pyroxenites is, on average, more Fe-rich than in intrusions of types I and II, but contains significant Ni (0.30–0.45 wt.% NiO). Olivine compositions in pyroxenites of types I, II and IV define a general trend of Fe-enrichment and Ni-depletion roughly compatible with olivine fractionation (Fig. 4). Fractionation processes could link olivine within composite vein S5–CV, orthopyroxenite S10–O (with the exception of one analysis), clinopyroxenite S2–C, and within orthopyroxenite S9–O to those in S8–O, and olivine from the rim (higher Ni-content) and core of orthopyroxenite S6–O. Olivine in type-III websterite S4–W is significantly more Fe-rich than in the other intrusions, and does not fall along the main olivine-fractionation trend. Contrary to inferences made from spinel and pyroxene chemistry, olivine in websterite S4–W is too Ni-rich to have it fractionated from a type-I orthopyroxenitic magma, like in the case of orthopyroxenite S9–O. However, type-III and type-IV dykes contain modal Fe–Ni sulfides, whereas type-I and type-II dykes do not. It is possible that postcumulus Ni-enrichment in olivine occurs within dykes that accumulated significant amounts of immiscible droplets of Fe–Ni sulfide.

WHOLE-ROCK CHEMISTRY

Major- and trace-element compositions of NAMM pyroxenite dykes (Tables 5, 6) reflect their modal mineralogy and the refractory composition of their minerals. Pyroxenite dykes have high Mg-numbers (between 0.88 and 0.92), high Ni (520–1650 ppm) and Cr contents (2600–6000 ppm), low Al_2O_3 (1.1–2.8 wt.%), Na_2O (0.02–0.24%), K_2O (0.03–0.08%) and TiO_2 (0.01–0.09%). They show, on average, a higher content in Al_2O_3 than pyroxenite dykes that belong to the low-Al Lewis Hills suite, whereas the clinopyroxene-rich dykes show Al_2O_3 contents similar to those of clinopyroxenite and websterite dykes that belong to the high-Al Lewis Hills suite (Edwards 1991; Fig. 5).

Type-I orthopyroxenites are characterized by low CaO and Al_2O_3 contents and high Mg# (Fig. 5). They are also characterized by a general trend, from orthopyroxenite S9–O to S3–O, of enrichment in Fe, Ca, Al, Na, Ti, V and Sc, coupled with Mg, Cr and Ni depletion (Fig. 5, Tables 5, 6) attributable to olivine ± spinel fractionation. Type-III websterite S4–W and websteritic composite vein S1–CV2 show lower Mg#, Cr and Ni contents and higher contents of Fe, Ca, Al, Na, Ti, V and Sc. They roughly fall along the type-I

TABLE 5. WHOLE-ROCK MAJOR-ELEMENT COMPOSITIONS, PYROXENITE DYKES, NORTH ARM MOUNTAIN MASSIF

Sample	S1-C1	S1-C2	S1-CV1	S1-CV2	S3-O	S4-W	S5-O	S5-CV	S6-O	S7-O	S8-O	S9-O	S10-O	S11-O	1d	1e
Type[1]	cpxite	cpxite	comp	comp	opxite I	webs	opxite II	comp[2]	opxite I	opxite I	opxite I	opxite I	opxite II	opxite II	harz [5]	lherz [5]
SiO_2 (wt.%)	49.03	48.76	44.27	50.51	52.19	51.54	49.58	52.32	50.57	49.27	52.07	47.96	49.79	49.32	37.57	38.77
TiO_2	0.09	0.05	0.03	0.04	0.03	0.04	0.04	0.03	0.02	0.04	0.02	0.02	0.02	0.01	0.01	0.02
Al_2O_3	2.78	1.85	1.70	1.63	1.33	1.48	2.77	1.10	0.90	0.95	1.11	0.63	1.57	1.69	0.57	1.38
Fe_2O_3*[3]	4.42	4.66	6.84	5.70	7.83	5.48	6.66	7.12	8.00	6.81	6.64	6.69	6.46	7.21	7.93	8.04
MnO	0.10	0.10	0.13	0.13	0.16	0.13	0.12	0.14	0.15	0.14	0.13	0.12	0.12	0.13	0.11	0.12
MgO	22.37	23.56	30.62	23.98	31.52	21.45	35.25	35.71	35.19	33.66	34.32	36.49	34.98	36.95	39.87	38.96
CaO	15.43	15.17	6.06	11.66	2.06	16.07	1.22	1.31	0.72	0.90	1.05	0.55	1.38	1.10	0.66	1.41
Na_2O	0.24	0.14	0.08	0.11	0.04	0.23	0.15	0.05	0.03	0.05	0.03	0.02	0.07	0.04	0.00	0.08
K_2O	0.06	0.05	0.05	0.04	0.05	0.07	0.06	0.07	0.06	0.06	0.05	0.05	0.08	0.03	0.00	0.00
P_2O_5	0.17	0.18	0.17	0.14	0.18	0.20	0.18	0.18	0.18	0.18	0.17	0.17	0.18	0.00	0.01	0.01
LOI	3.38	5.33	8.84	2.72	2.09	1.26	2.02	1.78	4.20	6.66	0.84	6.91	3.30	3.18	12.80	9.82
Total	99.19	100.97	99.63	97.22	98.20	98.92	98.97	100.70	100.62	99.46	97.31	100.64	99.04	99.66	99.52	98.60
Mg#[4]	90.93	90.92	89.86	89.28	88.85	88.57	91.29	90.85	89.70	90.73	91.10	91.53	91.47	91.03	90.70	90.56

nd: not determined (below detection limits); [1] see notes in Table 1; [2] orthopyroxenitic margin of composite vein S5-CV; [3] analysed total iron; [4] 100*Mg/(Mg + Fe^{2+}), Fe^{2+} as total iron; [5] average composition of harzburgites (NAMM unit 1d) and lherzolites (NAMM unit 1e).

TABLE 6. WHOLE-ROCK TRACE-ELEMENT CONCENTRATIONS, PYROXENITE DYKES, NORTH ARM MOUNTAIN MASSIF

Sample	S1-C1	S1-C2	S1-CV1	S1-CV2	S3-O	S4-W	S5-O	S5-CV	S6-O	S7-O	S8-O	S9-O	S10-O	S11-O	1d	1e
Type[1]	cpxite	cpxite	comp	comp	opxite I	webs	opxite II	comp[2]	opxite I	opxite I	opxite I	opxite I	opxite II	opxite II	harz [3]	lherz [3]
Sc (ppm)	47	51	26	46	21	49	22	12	9	13	11	8	19	-	-	-
V	190	162	90	160	83	160	114	51	34	48	49	39	84	-	27	54
Cr	4378	3698	3216	2664	3727	3505	4565	3827	2964	3423	5364	5802	6005	-	1389	1872
Ni	1085	1528	1647	604	818	519	1238	1385	942	805	803	1280	1282	-	2063	1946
Rb (ppb)	231	85	201	165	187	89	77	58	133	108	56	109	83	149	40	128
Sr	4425	5033	3303	2839	964	4143	382	433	719	1144	431	636	606	453	823	683
Zr	1532	865	1181	742	903	725	129	131	632	293	760	299	310	324	99	42
Nb	59	55	45	45	14	50	34	38	44	12	42	58	29	13	40	24
Cs	59	13	74	36	25	22	19	11	32	47	9	70	47	187	10	19
Ba	357	590	640	2246	4319	176	1043	170	1135	2950	1990	1133	850	1530	965	449
La	nd	42.8	146.9	60.8	390.3	nd	nd	nd	263.0	66.0	356.4	193.4	223.8	886.5	70.0	3.8
Ce	nd	174.6	553.1	235.7	1422.9	5.0	nd	nd	886.1	257.5	1242.3	660.6	583.8	1714.3	126.9	31.0
Pr	65.0	48.2	42.8	42.4	21.4	50.9	1.4	3.5	14.8	4.6	16.9	9.0	28.8	147.0	10.7	0.6
Nd	315.8	182.2	179.5	165.2	63.9	180.7	6.4	12.6	45.4	10.9	51.0	26.0	70.7	358.6	31.6	7.7
Sm	202.3	110.2	62.3	68.1	16.0	71.1	4.6	5.8	9.7	5.1	8.8	5.8	4.3	2.8	3.8	4.9
Eu	83.1	44.1	22.7	24.0	4.0	24.8	1.8	1.8	1.5	0.6	0.4	nd	0.9	0.4	0.1	1.4
Gd	426.5	213.7	101.2	106.5	33.4	107.8	12.0	10.1	25.2	9.0	31.3	16.3	5.8	nd	4.8	10.2
Tb	91.0	43.9	20.4	23.1	6.0	22.9	4.2	3.0	2.2	2.0	2.5	0.9	1.1	0.1	0.6	3.6
Dy	685.0	341.5	159.5	189.3	54.7	180.6	46.7	31.4	19.9	19.0	20.9	9.3	13.4	8.3	4.9	37.3
Ho	153.2	75.1	36.2	45.2	14.4	43.0	13.9	8.5	5.1	5.8	5.6	2.7	4.2	1.5	1.1	10.6
Er	463.1	231.6	121.6	148.5	55.7	144.6	57.3	34.2	20.6	25.1	23.2	11.5	22.5	14.2	5.7	40.9
Tm	67.0	33.6	19.8	24.7	10.2	23.3	11.0	6.6	4.2	5.1	4.7	2.5	5.1	3.6	1.2	7.8
Yb	420.1	216.1	136.4	168.2	83.9	167.4	94.9	53.0	33.0	42.8	39.2	20.3	49.8	36.0	11.3	61.7
Lu	66.0	34.5	23.6	30.3	16.2	29.3	18.1	10.3	6.8	8.6	8.1	4.2	10.8	8.7	2.9	12.1
Hf	78.9	37.7	38.2	32.2	25.0	32.4	4.3	4.4	14.5	7.5	17.2	6.9	6.5	7.3	1.3	2.0
Ta	nd	nd	nd	nd	nd	nd	nd	nd	0.2	nd	nd	0.4	nd	nd	0.6	0.0
Th	1.7	2.0	4.0	8.3	8.0	0.8	0.1	0.6	11.0	4.5	5.7	4.0	7.5	3.6	1.1	0.9
U	2.6	1.5	1.8	1.4	1.6	1.2	1.9	0.8	3.4	1.7	1.0	1.2	3.9	0.9	1.1	0.9

nd: not determined (below detection limits); [1] see notes in Table 1; [2] orthopyroxenitic margin of composite vein S5-CV;
[3] average composition of harzburgites (NAMM unit 1d) and lherzolites (NAMM unit 1e).

orthopyroxenite trends for these elements, and so could be related to them by fractional crystallization, which is consistent with inferences made from spinel and pyroxene chemistry. On the other hand, type-II orthopyroxenites S5–O, S10–O and S11–O are characterized by high Mg# and low CaO, but are principally distinguished from type-I orthopyroxenite by their high Al_2O_3 contents (Fig. 5), although they also show slightly higher contents in Na_2O, CaO, Ni, Sc and V. The orthopyroxenitic margin of type-II composite vein S5–CV shows a high Mg# and Ni content, and slightly higher CaO content, like the other type-II orthopyroxenites, but Sc and V contents similar to type-I orthopyroxenites. Its Al_2O_3 and Na_2O contents are between those of types-I and -II orthopyroxenites. Type-IV clinopyroxenites S1–C, S1–C2 and composite vein S1–C1 are distinguished from type-III pyroxenites by their high Al_2O_3 contents coupled with their high Mg# and Ni contents, supporting observations made from mineral chemistry. Clinopyroxenites S1–C1 and S1–C2 also show a slightly higher TiO_2 content than the other pyroxenites.

NAMM intrusive pyroxenites contain low concentrations of incompatible trace elements, generally between 3 and 0.01 times chondritic values, and strong depletions in Ta (Table 6, Fig. 6). Trace-element patterns among the NAMM pyroxenite dykes are of two sorts: type-I and type-II orthopyroxenitic dykes show

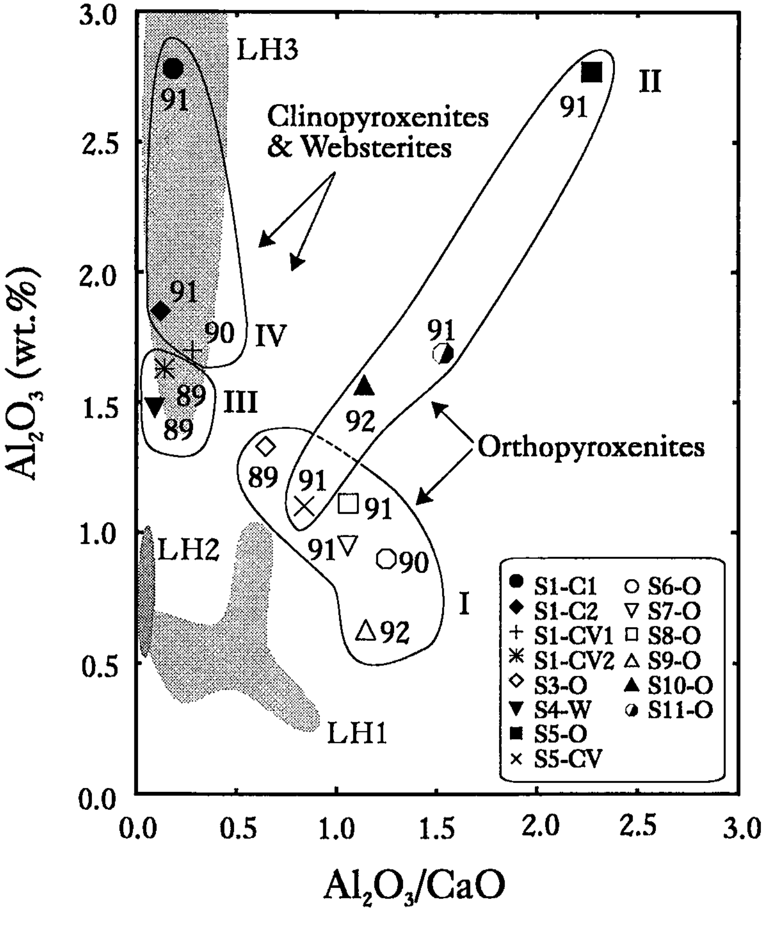

FIG. 5. Whole-rock Al_2O_3 content *versus* Al_2O_3/CaO wt.% ratios of pyroxenite dykes. Dashed fields enclose suites of type-I, type-II, type-III and type-IV pyroxenite dykes. Numbers near symbols represent Mg# values of pyroxenite dykes [Mg# = 100 × Mg/(Mg + Fe^{2+}), total iron as Fe^{2+}]. Also shown are data (grey fields) for Lewis Hills massif orthopyroxenite dykes of the low-Al suite (LH1), olivine clinopyroxenite, clinopyroxenite and websterite dykes of the low-Al suite (LH2), and olivine clinopyroxenite dykes of the high-Al suite (LH3), from Edwards (1991) and Edwards & Malpas (1995).

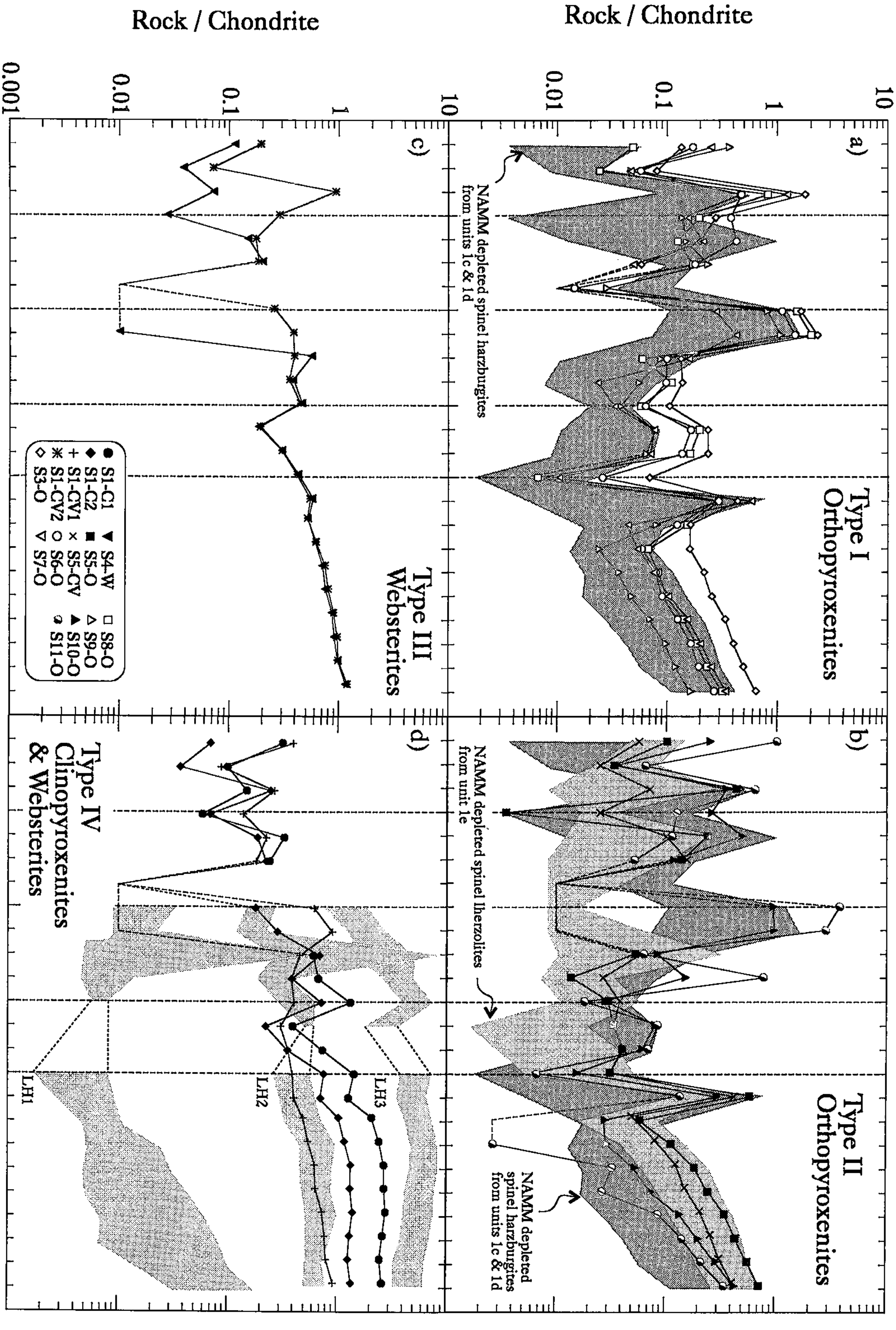
Rock / Chondrite
Rock / Chondrite
10
1
0.1
0.01
0.001
a)
Type I Orthopyroxenites
NAMM depleted spinel harzburgites from units 1c & 1d
b)
Type II Orthopyroxenites
NAMM depleted spinel lherzolites from unit 1e
NAMM depleted spinel harzburgites from units 1c & 1d
c)
Type III Websterites
d)
Type IV Clinopyroxenites & Websterites
LH1
LH2
LH3
Cs Rb Ba Th U Nb Ta La Ce Sr Nd Sm Zr Hf Eu Ti Gd Tb Dy Ho Er Tm Yb Lu
● S1-C1 ▼ S4-W □ S8-O
◆ S1-C2 ■ S5-O △ S9-O
+ S1-CV1 × S5-CV ▲ S10-O
✳ S1-CV2 ○ S6-O ◐ S11-O
◇ S3-O ▽ S7-O

U-shaped patterns relative to chondritic values, with strong $[MREE/HREE]_N$ fractionation (*MREE*: middle rare-earth elements, such as Sm and Eu, *HREE*: heavy rare-earth elements, such as Yb and Lu) and relatively high *LILE* contents (large-ion lithophile elements, such as Rb, Ba, Th and U); types-III and -IV clinopyroxene-rich dykes show flatter to concave-downward trace-element patterns, with near-chondritic values and less important relative *LILE* and *LREE* (light rare-earth elements, such as La and Ce) enrichments, compared to orthopyroxenitic dykes.

Type-I orthopyroxenites are characterized by strongly fractionated U-shaped *REE* patterns relative to chondritic values: their $[La/Sm]_N$ values range between 8 and 26, their $[Eu/Yb]_N$ values are ≤0.14, and their $[Tb/Yb]_N$ values range between 0.21 and 0.33 (Fig. 6a). The normalized *REE* profiles of S9–O, S8–O and S6–O are also characterized by a positive anomaly for Gd relative to Tb. Normalized profiles for type-I orthopyroxenite are also characterized by strong positive anomalies for Zr, Hf, and Ti relative to the *MREE*. Type-I orthopyroxenites form a set of roughly parallel normalized patterns, orthopyroxenite S9–O showing the lowest concentrations, and S3–O orthopyroxenite, the highest (among the type-I suite). This trend is consistent with fractional crystallization, supporting inferences made from mineral chemistry and major- and transition-element chemistry. The concordance between chondrite-normalized patterns for type-I orthopyroxenite and those of depleted hosting harzburgites from NAMM units 1c and 1d is noteworthy, though the absolute trace-element abundances in orthopyroxenites are slightly higher than in the host harzburgites. Patterns for type-1 orthopyroxenite are comparable, although at significantly higher trace-element abundances, to those of the low-Al Lewis Hills orthopyroxenite dykes (Edwards 1991; Fig. 6c).

Type-II orthopyroxenites S10–O and S11–O have very similar chondrite-normalized profiles to those of the type-I suite (Fig. 6b). They are characterized by strongly fractionated U-shaped *REE* patterns relative to chondritic values, and by strongly positive anomalies for Zr, Hf, and Ti relative to the *MREE*. They are, however, characterized by an even more strongly fractionated *REE* pattern relative to chondrite: their $[La/Sm]_N$ values are respectively (S10–O and S11–O) 33 and 203, their $[Eu/Yb]_N$ values are 0.06 and 0.03, and their $[Tb/Yb]_N$ values, 0.10 and 0.02. Their normalized *REE* profile also distinguish them from those of the type-I suite by a positive anomaly for Nd relative to Sm. Type-II orthopyroxenite S5–W has higher *MREE*, *HREE* and Ti contents than S10–O and S11–O orthopyroxenites but has, like them, a strongly fractionated chondrite-normalized profile for these elements, showing a strong positive anomaly for Ti relative to *MREE*, a low $[Eu/Yb]_N$ value of 0.05, and a low $[Tb/Yb]_N$ value of 0.20. Orthopyroxenite S5–O, however, differs from the other type-I and type-II orthopyroxenites by having a $[La/Sm]_N$ value less than 1 and by not showing significant Zr and Hf anomalies relative to the *MREE*. The chondrite-normalized profile of the orthopyroxenitic margin of the type-II composite vein S5–CV is remarkably similar to that of orthopyroxenite S5–O, though it has slightly lower *HREE* contents and a slightly less fractionated *HREE* profile, with a $[Eu/Yb]_N$ value of 0.10 and a $[Tb/Yb]_N$ value of 0.26. The concordance between chondrite-normalized patterns for type-II orthopyroxenites S5–O and S5–CV and those of the depleted host lherzolites from NAMM unit le is noteworthy, depleted lherzolites of unit 1e showing higher *HREE* contents than the NAMM harzburgites, with more fractionated $[MREE/HREE]_N$ profiles, and no La and Ce enrichment (Varfalvy *et al.* 1995).

Type-III websterite S4–W and composite vein S1–CV2 are characterized by $[La/Sm]_N$ values less than 1 and moderately fractionated *MREE* and *HREE* patterns at near chondritic values, with $[Eu/Yb]_N$ values of 0.43 and 0.42, respectively, and $[Tb/Yb]_N$ values of 0.62 (Fig. 6c). They are also characterized by moderate negative anomalies for Zr and Hf relative to the *MREE*. They resemble clinopyroxenite and websterite dykes of the low-Al Lewis Hills suite (Edwards 1991; Fig. 6d). Type-IV clinopyroxenites S1–C1 and S1–C2 display concave-downward chondrite-normalized patterns (Fig. 6d), with trace-element abundances higher than in the pyroxenites described above. They both show nearly flat *HREE* profiles, with $[Tb/Yb]_N$ values of 0.99 and 0.92, respectively, moderately fractionated $[MREE/HREE]_N$ profiles, with $[Eu/Yb]_N$ values of 0.58 and 0.60, respectively, and $[La/Sm]_N$ values less than 1 (Fig. 6d). They are also characterized by negative anomalies for Zr, Hf and Ti relative to the *MREE*. Their normalized profiles resemble, at lower *REE* contents, those of clinopyroxenite dykes that belong to the high-Al Lewis Hills suite (Edwards 1991; Fig. 6d). Type-IV composite vein S1–CV1 presents a slightly concave-upward chondrite-normalized pattern, with $[La/Sm]_N$, $[Eu/Yb]_N$ and $[Tb/Yb]_N$ values of 1.52, 0.49 and 0.68, respectively (Fig. 6d). It has trace-element abundances very similar to those of the type-III pyroxenites described above, without Zr, Hf or Ti anomalies relative to the *MREE*, however.

FIG. 6. Chondrite-normalized *REE* abundance patterns for a) type-I orthopyroxenite dykes, b) type-II orthopyroxenite dykes, c) type-III websterite dykes, and d) type-IV clinopyroxenite and websterite dykes. Also shown are data fields for NAMM host depleted spinel harzburgites from units 1c and 1d [background dark grey field in a) and b)], NAMM host depleted spinel lherzolites from unit 1e [pale grey field in b)] and Lewis Hills massif pyroxenite dykes, from Edwards (1991) and Edwards & Malpas (1995) (grey fields in d); see caption to Figure 5. Dashed lines link values below detection limits. Normalization values to chondrite C1 are from Sun & McDonough (1989).

NATURE OF RELATED MAGMAS

The NAMM pyroxenitic dykes and their constituent minerals are characterized by low contents of Al, Na, K, Ta, Zr, Hf, Ti and the *REE*, high Mg-numbers, high Cr and Ni contents, and *LILE* enrichment relative to less incompatible elements. Liquids calculated to be in equilibrium with olivine and the pyroxenes in these pyroxenite dykes have high Mg-numbers, comprised between 0.64 and 0.78 (Varfalvy *et al.* 1996). These Mg-numbers are much higher than those of natural primitive MORB glasses, which are rarely greater than 0.65 (Sinton & Detrick 1992). Mg-numbers greater than 0.65 are more characteristic of subduction-related basalts (Hawkins 1977, 1980), and are usually interpreted to result from remelting of a depleted mantle-wedge source (Pearce 1982, Duncan & Green 1987). The calculated Ni content of liquids inferred to be in equilibrium with olivine of the NAMM pyroxenite dykes varies from 120 to 400 ppm (Varfalvy *et al.* 1996; see caption to Fig. 4 for K_d used). Such high Ni contents are not typical of oceanic ridges, since MAR basalts average 123 ppm Ni (Hawkins 1977). Ni contents greater than 200 ppm are more commonly observed in island-arc tholeiites, backarc tholeiites, subduction-related magnesian quartz tholeiites and highly magnesian andesites, including typical boninites (Hawkins 1977, Beccaluva & Serri 1988, Crawford *et al.* 1990). The high Mg-numbers and Ni contents of liquids from which the NAMM intrusive pyroxenites precipitated, coupled with their refractory chemistry and strongly depleted trace-element abundances, support the hypothesis that the relevant magmas were generated in a supra-subduction-zone environment. The absence of amphibole in most NAMM pyroxenite dykes does not necessarily imply a dry system. The high temperatures recorded in the pyroxenes (1050°–1100°C; single pyroxene geothermometer of Mercier 1980) likely reflect the minimum ambient temperature of the upper mantle during pyroxenite emplacement (Varfalvy *et al.* 1996). We suggest that amphiboles may not have formed, even if the magma was hydrous, because temperatures were too high (Boyd 1959, Kushiro *et al.* 1968, Green 1973, Jenkins 1983).

Textural observations, and whole-rock and mineral compositional variations, suggest that the magmas that formed the NAMM pyroxenites initially had olivine, orthopyroxene and chromian spinel on the liquidus, and that fractionation of these phases led to progressive enrichment in Ca and eventual saturation in clinopyroxene. The zonation of pyroxenite intrusions from an olivine- and orthopyroxene-rich margin to a clinopyroxene-rich core supports this sequence of crystallization. This early precipitation of orthopyroxene implies that the liquids from which most NAMM pyroxenites precipitated were saturated to oversaturated in silica (Morse 1980, Kushiro 1969) and likely had an andesitic SiO_2 content, greater than 55 wt.% (Varfalvy *et al.* 1996).

In order to better study the melts related to the NAMM pyroxenites and compare these with lavas, we use the inferred composition of liquids that were in equilibrium with these pyroxenites, obtained by mass-balance calculations according to the method of Bédard (1994). We used the partition coefficients compiled by Bédard (1994). The calculations involve a trapped melt component. Textural and mineralogical data allow the trapped melt fraction to be constrained. Specifically, there is a low modal proportion of interstitial clinopyroxene in the orthopyroxenites, and Fe–Ni sulfides or retrograde amphiboles, where present, form less than 1% of the rocks. On the basis of these observations, we assumed the trapped melt component for the calculations to be 1% in the NAMM intra-mantle pyroxenitic intrusions. The normative compositions used for the calculations is made of variable proportions of olivine, orthopyroxene, clinopyroxene and chromian spinel. Calculations show that the trace-element contents of the calculated melt increase with a decrease in the assumed amount of trapped melt, or with an increase in the proportion of modal orthopyroxene to clinopyroxene and olivine to clinopyroxene (Fig. 7). However, the largest source of error may lie in the value of the solid/liquid partition coefficients that were used. The crystal/liquid partition coefficient for orthopyroxene is poorly known. Use of lower partition coefficients of the *REE* for orthopyroxene, like those proposed by Kelemen *et al.* (1990), increases the absolute abundance of trace elements of the calculated equilibrium melt, but do not change the shape of the profile to any significant degree (Fig. 7). Although data on partition coefficients for olivine and spinel are also highly variable, these minerals are modally less abundant than the pyroxenes, and so do not affect the shape of the calculated profiles of the liquid to the same extent. Crystal/liquid partition coefficient values for the *LILE* also are poorly known; there is a vast range of experimentally determined values of partition coefficients for the *LILE* elements in olivine, the pyroxenes and spinel; the olivine/liquid and orthopyroxene/liquid partition coefficients used for Ba, Nb, Rb and Cs were simply assumed by Bédard (1994). Moreover, the effect of serpentinization on these elements, and the *LREE* as well, may be important (considering that they are potentially more mobile), but is not well understood (Parkinson *et al.* 1992). However, we do not observe any significant correlation between these elements and loss on ignition (taken as an index of the degree of serpentinization) among the NAMM dykes. We assume, then, that these elements were not affected by serpentinization, and that the calculated *LILE* and *LREE* contents likely reflect those of melts related to the NAMM pyroxenites. Chondrite-normalized calculated trace-element concentrations of melts inferred to be in equilibrium with the NAMM pyroxenites are presented in Figure 8.

Liquids calculated to be in equilibrium with type-I and type-II orthopyroxenitic dykes of the NAMM suite have extremely low *MREE*, *HREE*, Ta, Zr, Hf and Ti abundances, that range between 0.1 to 3 times chondrite values; they present U-shaped chondrite-normalized patterns, with moderate to strong $[MREE/HREE]_N$ fractionation and an important *LILE* enrichment relative to less incompatible elements. They are all characterized by a strong positive anomaly for Ti relative to the *MREE*, and a strong depletion in Ta. The chondrite-normalized *REE* profiles of melts related to type-I orthopyroxenites are characterized by $[La/Sm]_N$ values of ~20–65, $[Eu/Yb]_N$ values of ~0.1–0.5, and $[Tb/Yb]_N$ values of ~0.5–0.8 (Fig. 8a). *REE* profiles of melts related to S9–O, S8–O and S6–O are also characterized by a positive anomaly for Gd relative to Tb. Melts related to type-II orthopyroxenites S10–O and S11–O are very similar to those related to type-I orthopyroxenites, but show more fractionated *REE* patterns relative to chondrite, with $[La/Sm]_N$ values of ~80–460, $[Eu/Yb]_N$ values of ~0.1–0.2, and $[Tb/Yb]_N$ values of ~0.1–0.3 (Fig. 8b). These *REE* profiles also are distinct from those of the type-I suite by a positive anomaly for Nd relative to Sm. Melts related to type-II orthopyroxenitic dykes S5–O and S5–CV (its orthopyroxenitic margins) present moderately fractionated chondrite-normalized *REE* profiles characterized by $[Eu/Yb]_N$ values of ~0.2–0.3 and $[Tb/Yb]_N$ values of ~0.5–0.6 (Fig. 8b). We estimate that the $[La/Sm]_N$ values of the liquids should be equal to or less than 1, since whole rocks with La and Ce abundances 0.01 times chondrite (the detection limit for La and Ce) would yield calculated liquids with chondritic La and Ce abundances. Calculated melts in equilibrium with NAMM orthopyroxenitic dykes reflect fairly well the trace-element chemistry of the rocks, with, however,

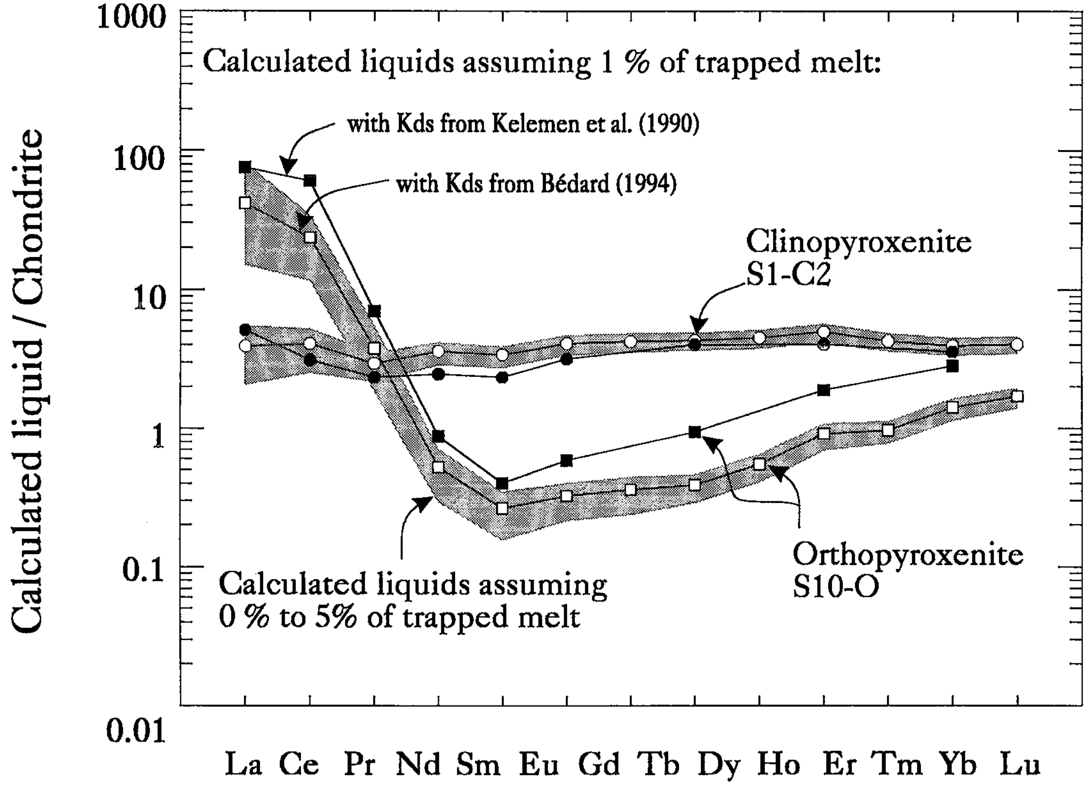

FIG. 7. Chondrite-normalized *REE* abundance patterns representing calculated magmas in equilibrium with two samples of NAMM pyroxenite: clinopyroxenite S1–C2 (circles) and orthopyroxenite S10–O (squares). *REE* abundance patterns are calculated according to the method described in Bédard (1994), assuming 1% of trapped melt. Partition coefficients for olivine, orthopyroxene, clinopyroxene and spinel are from Bédard (1994) (open symbols) and Kelemen *et al.* (1990) (filled symbols). The grey fields represent, for clinopyroxenite S1–C2 and orthopyroxenite S10–O respectively, calculated normalized abundances in liquid, with the assumed trapped melt component varying from 0% (upper limits) to 5% (lower limits); partition coefficients used are from Bédard (1994). Normalization values of chondrite C1 are from Sun & McDonough (1989).

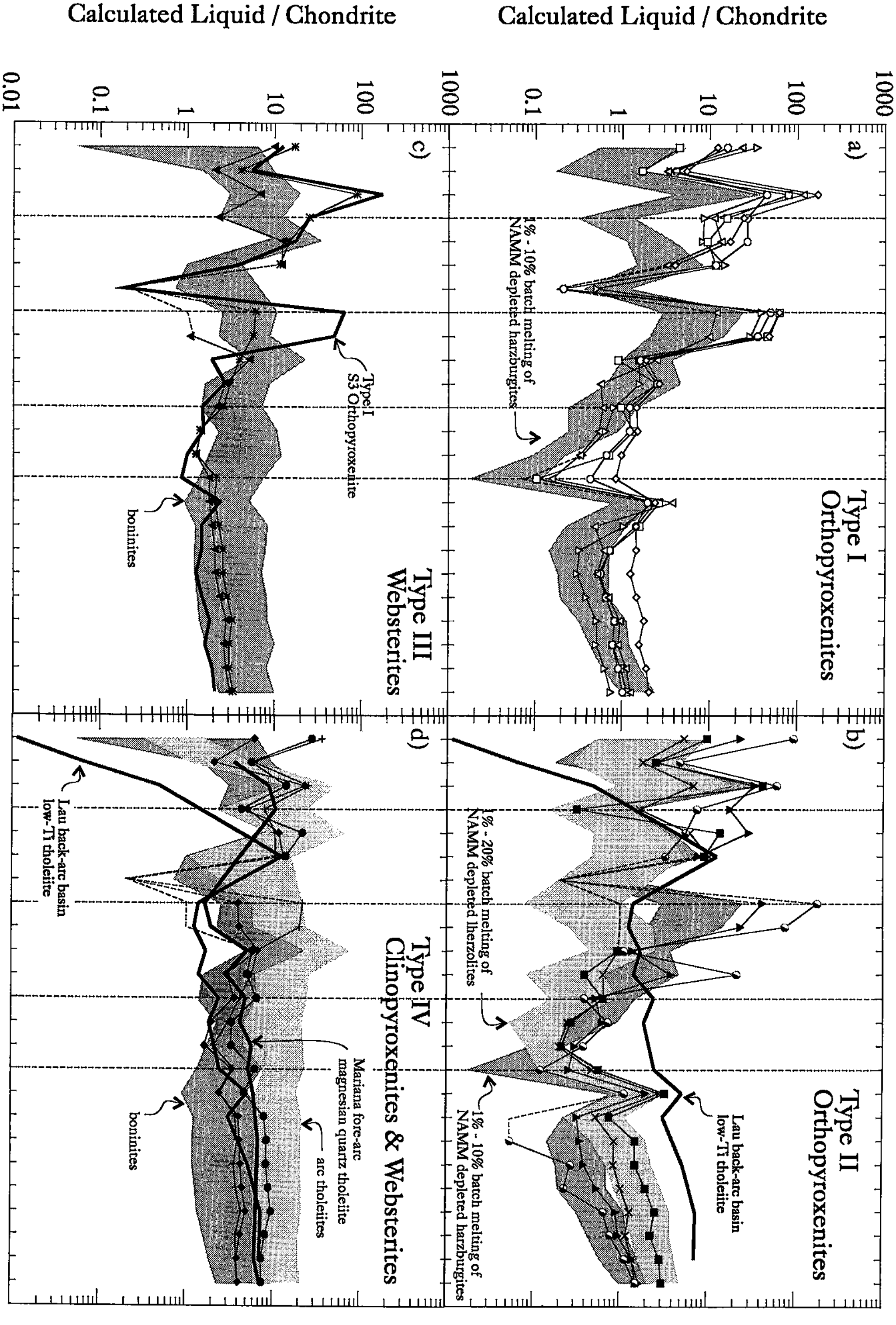
Calculated Liquid / Chondrite
Calculated Liquid / Chondrite
1000
100
10
1
0.1
0.01
a)
Type I Orthopyroxenites
1% - 10% batch melting of NAMM depleted harzburgites
b)
Type II Orthopyroxenites
Lau back-arc basin low-Ti tholeiite
1% - 20% batch melting of NAMM depleted lherzolites
1% - 10% batch melting of NAMM depleted harzburgites
c)
Type III Websterites
Type I S3 Orthopyroxenite
boninites
d)
Type IV Clinopyroxenites & Websterites
Lau back-arc basin low-Ti tholeiite
Mariana fore-arc magnesian quartz tholeiite
arc tholeiites
boninites
Cs Rb Ba Th U Nb Ta La Ce Sr Nd Sm Zr Hf Eu Ti Gd Tb Dy Ho Er Tm Yb Lu
Cs Rb Ba Th U Nb Ta La Ce Sr Nd Sm Zr Hf Eu Ti Gd Tb Dy Ho Er Tm Yb Lu

the exception of the positive Zr and Hf anomalies relative to the *MREE*, that become subtle to absent in the calculated liquids.

Liquids calculated to be in equilibrium with type-III websterite S4–W and websteritic composite vein S1–CV2 have low *MREE*, *HREE*, Ta, Zr, Hf and Ti abundances, that range between 1 to 3 times chondritic values, and present concave-upward chondrite-normalized patterns, with slight $[MREE/HREE]_N$ fractionation and a relative *LILE* enrichment (Fig. 8c). They are also characterized by a strong depletion in Ta and slight negative anomalies for Zr and Hf relative to the *MREE*. Their *REE* chondrite-normalized profiles are characterized by $[La/Sm]_N$ values ≤2.0, $[Eu/Yb]_N$ values of ~0.6–0.7, and $[Tb/Yb]_N$ values of ~0.75–0.85. They have variable *LILE* enrichment relative to less incompatible elements; melt related to composite vein S1–C2 show a more important relative *LILE* enrichment than S4–W websterite, trending to abundances characteristic of melts related to type-I orthopyroxenites. The abundance of *REE*, Zr, Hf and Ti of these calculated melts is well below (0.2 to 0.5 times) typical N–MORB values from Sun & McDonough (1989). Nor are such low *HREE* abundances typical of arc tholeiites and low-Ti subduction-related basalts (Pearce 1982, Beccaluva & Serri 1988); these rarely exhibit *MREE* and *HREE* abundances lower than five times chondritic values. Only boninites have such low *HREE* contents (Kuroda *et al.* 1978, Cameron *et al.* 1979, 1983, Jenner 1981, Hickey & Frey 1982, Walker & Cameron 1983, Umino 1985, 1986, Beccaluva & Serri 1988, Crawford *et al.* 1990, Taylor *et al.* 1994). Melts related to type-III websterites and to the most evolved member of the type-I suite, S3–O orthopyroxenite, show trace-element patterns very close to those of modern boninites, but not identical to them, since they do not exhibit positive Sr, Zr and Hf anomalies, and negative Nb and Ti anomalies observed in boninites (Fig. 8c). Moreover, melts related to type-I orthopyroxenite S3–O and to type-III composite vein S1–CV2 tend to have higher *LILE* enrichment than boninites, whereas the melt related to type-III websterite S4–W has a lower $[La/Sm]_N$ value.

Melts calculated to be in equilibrium with type-IV clinopyroxenites S1–C1 and S1–C2 and websteritic composite vein S1–CV1 show very similar concave-upward trace-element patterns, with slight $[MREE/HREE]_N$ fractionation and relative *LILE* enrichment (Fig. 8d). They are also characterized by a strong depletion in Ta, and negative anomalies for Zr, Hf and Ti relative to the *MREE*. Their chondrite-normalized *REE* profiles are characterized by $[Eu/Yb]_N$ values of ~0.8–0.9, $[Tb/Yb]_N$ values of ~1.0, and variable $[La/Sm]_N$ values (≤1.0 for melts related to the clinopyroxenites and ~5 for melt related to S1–CV1 composite vein). The abundance of *MREE*, *HREE*, Zr, Hf and Ti of these calculated melts is between two and nine times chondritic values (~0.05 to 0.5 N-MORB values). Such low abundances of the *HREE* are not common for arc tholeiites; ultra-depleted low-Ti subduction-related tholeiites, such as those found in the Lau backarc basin (Hawkins & Melchior 1985), will generally present more fractionated *REE* profiles (Fig. 8d). Magmas related to the type-IV pyroxenites, which are, at higher abundances, very close to those of type-III pyroxenites, resemble modern boninites (Fig. 8d). However, they are not identical to them, since they exhibit significantly negative Zr and Hf anomalies (a feature observed in many island-arc tholeiites: Dupuy *et al.* 1982), instead of the positive Zr and Hf anomalies observed in boninites. Moreover, they do not show a negative Nb anomaly. On the other hand, melt calculated to be in equilibrium with type-IV clinopyroxenite S1–C1, which has *HREE* abundances higher than other NAMM pyroxenites and a lower $[La/Sm]_N$ value than that of typical boninites, may be comparable to highly depleted magnesian quartz-normative arc tholeiites found at the Mariana fore-arc and the Yap trench intersection. These rocks are mineralogically and chemically transitional between typical primitive island-arc tholeiites and typical boninites (Beccaluva & Serri 1988; Fig. 8d).

FIG. 8. Chondrite-normalized abundance patterns for calculated magmas in equilibrium with a) type-I orthopyroxenite dykes, b) type-II orthopyroxenite dykes, c) type-III websterite dykes, and d) type-IV clinopyroxenite and websterite dykes, assuming 1% of trapped melt. Grey fields in a) and b) are drawn from calculated liquids resulting from 1% (upper limit) to 10% (lower limit) batch melting of average NAMM depleted spinel harzburgites from unit 1d (background dark grey field), and 1% (upper limit) to 20% (lower limit) batch melting of average NAMM depleted spinel lherzolites from unit 1e (pale grey field). The Lau basin tholeiite is from Gill (1976), Hawkins & Melchior (1985) and Beccaluva & Serri (1988). The arc-type magnesian quartz tholeiite is from the Mariana fore-arc and Yap Trench intersection (1438C, Crawford *et al.* 1986, Beccaluva *et al.* 1986, Beccaluva & Serri 1988). The boninite field (background dark grey field in Figs. 8c and 8d) is drawn from boninites from Bonin Islands (Taylor *et al.* 1994), and Izu–Bonin fore-arc (Murton *et al.* 1992). The arc tholeiite field is drawn from basalts from the Bismarck island arc (Basaltic Volcanism Study Project 1981). Dashed lines link up values below detection limits. Normalization values of chondrite C1 are from Sun & McDonough (1989). Symbols are the same as on Figure 6.

ORIGIN AND EVOLUTION OF RELATED MAGMAS

Nature of mantle sources

No known lavas have *HREE* contents as low as the liquids calculated to be in equilibrium with most of the NAMM orthopyroxenitic dykes. Such low *HREE* abundances indicate the extremely depleted character of their mantle source(s). Such depleted magmas could result from second-stage, or even third-stage melting of ultra-depleted mantle sources at shallow depths in the presence or absence of an H_2O-rich fluid, as proposed by Duncan & Green (1987). To a first approximation (and according to this model), NAMM lherzolites and harzburgites have extremely depleted geochemical signatures (with regard to the moderately incompatible elements, but not to the *LILE*) that may be interpreted as the result of respectively ~25–30% to more than 40% multiple-stage melt extraction from MORB-related pyrolite. The high Ni and Cr contents and Mg-numbers of the orthopyroxenite dykes, coupled with the similarity of their mineral chemistry to that of the host peridotites, are all consistent with the hypothesis that they are re-melts of depleted NAMM harzburgites and lherzolites. The high MgO and SiO_2 contents estimated for these NAMM melts are also consistent with this hypothesis, since magmas produced by shallow-level, hydrous partial melting of depleted peridotites will tend to have higher SiO_2 and MgO contents than those produced by dry melting of more fertile peridotites (O'Hara 1968, Elthon & Scarfe 1984, Fujii & Scarfe 1985, Duncan & Green 1987, Hirose & Kushiro 1993). This hypothesis is in agreement with the general interpretation for the genesis of magnesian quartz tholeiites to highly magnesian andesites, including boninites, which are considered to represent re-melts of variously depleted mantle sources in subduction environments (Kuroda *et al.* 1978, Cameron *et al.* 1979, 1983, Jenner 1981, Pearce 1982, Hickey & Frey 1982, Walker & Cameron 1983, Umino 1985, 1986, Duncan & Green 1987, Beccaluva & Serri 1988, Crawford *et al.* 1990, Kostopoulos 1991, Taylor *et al.* 1994).

To test this hypothesis for the NAMM dykes, we generated a series of model liquids by batch melting of NAMM mantle peridotites. Batch melts of depleted NAMM spinel harzburgites from unit 1d (average composition, Tables 5 and 6), and of depleted spinel

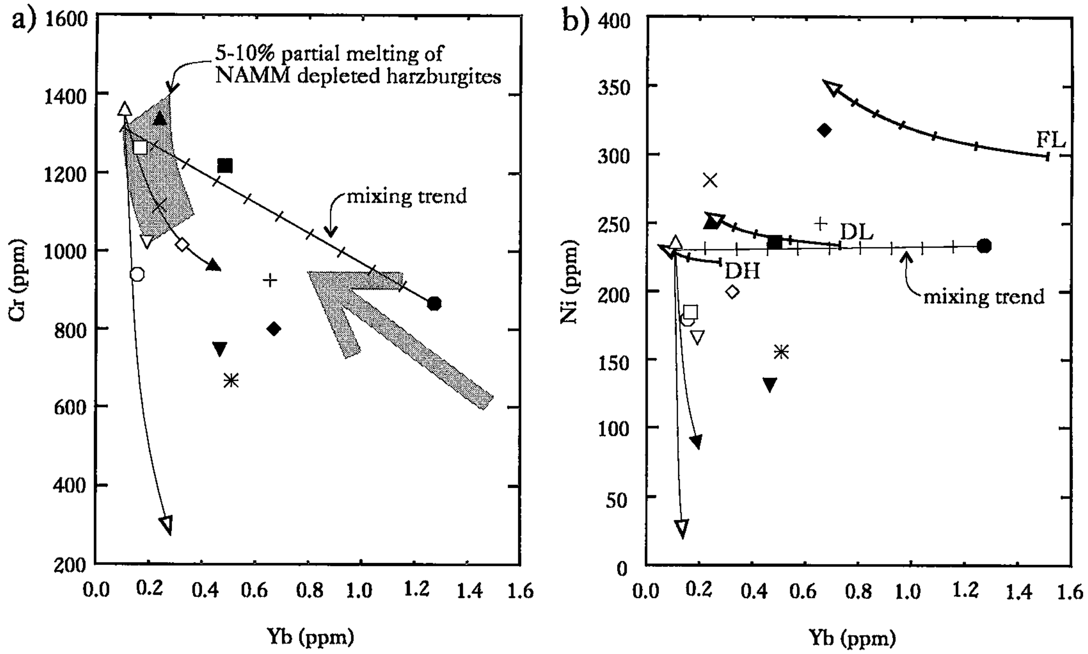

FIG. 9. a) Concentrations of Cr *versus* Yb and b) of Ni *versus* Yb (all in ppm) in calculated magmas in equilibrium with pyroxenite dykes, assuming 1% of trapped melt. The grey field in a) is drawn from calculated liquids resulting from 5% to 10% batch melting of NAMM depleted spinel harzburgites. The large grey arrow indicates the approximate direction of increasing partial melting of the mantle. Scaled arrows in b) represent calculated melts for 10–40% partial melting of average Balmuccia fertile spinel lherzolite (FL), 1–20% partial melting of average NAMM depleted spinel lherzolite from unit 1e (DL), and 1–10% partial melting of average NAMM depleted spinel harzburgite from unit 1d (DH). Scaled curves represent mixing trend between a liquid produced by 10% partial melting of average NAMM depleted spinel harzburgite from unit 1d, and calculated liquid in equilibrium with S1–C1 clinopyroxenite. White arrows are calculated olivine ± spinel (99:1) Rayleigh fractionation curves from a) 0–60% and b) 0–20% crystallization. Black arrows are calculated clinopyroxene assimilation – olivine ± spinel (99:1) fractionation curves from a) 0–80% and b) 0–20% of crystallization; we assume that the mass of the magma stays constant. Symbols are the same as on Figure 6.

lherzolites from unit 1e (average composition, Tables 5 and 6), are shown on Figures 8, 9 and 10. Batch melts of N-MORB-like fertile spinel lherzolites from Balmuccia (average composition; data are from Hartmann & Wedepohl 1993) are also shown on Figures 9 and 10. The terminology used for peridotites is after Kostopoulos (1991) and refers to different regimes of mantle melting. Melting proportions are $Ol_{0.01}Opx_{0.08}Cpx_{0.765}Spl_{0.145}$ for fertile spinel lherzolite, $Ol_{0.13}Opx_{0.85}Spl_{0.02}$ for depleted spinel harzburgite, and $Ol_{0.10}Opx_{0.64}Cpx_{0.24}Spl_{0.02}$ for depleted spinel lherzolite (Kostopoulos 1991). Equilibrium partial melting equations are from Allègre & Minster (1978). Partition coefficients for olivine, orthopyroxene, clinopyroxene and spinel are from Bédard (1994), with the exception of the ${}^{ol}D_{Ni}$, which was assumed to be constant and equal to 10.

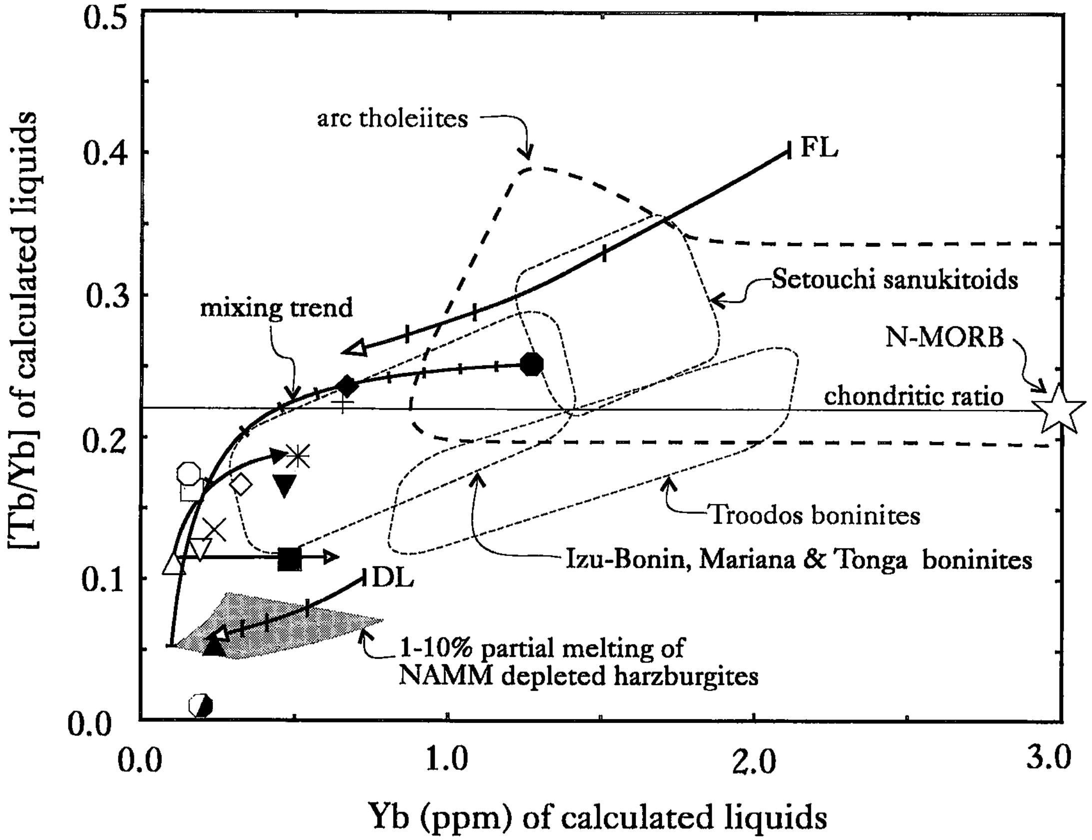

FIG. 10. Values of [Tb/Yb] *versus* concentration of Yb (ppm) of calculated magmas in equilibrium with pyroxenite dykes, assuming 1% of trapped melt. Scaled arrows represent calculated melts for 1–40% partial melting of average Balmuccia fertile spinel lherzolite (FL) and 1–20% partial melting of average NAMM depleted spinel lherzolite from unit 1e (DL). The grey field is drawn from calculated liquids resulting from 1 to 10% batch melting of NAMM depleted spinel harzburgites. The scaled curve represents a mixing trend between a liquid produced by 10% partial melting of average NAMM depleted spinel harzburgite from unit 1d, and calculated liquid in equilibrium with S1–C1 clinopyroxenite. The white arrow is a calculated olivine ± spinel (99:1) Rayleigh fractionation curve from 0 to 100% crystallization. The black arrow is calculated clinopyroxene assimilation – olivine ± spinel (99:1) fractionation curve from 0 to 100% crystallization. Also shown are data fields for: sanukoids from Setouchi volcanic belt (Tatsumi & Ishizaka 1982), boninites from Bonin Islands (Hickey & Frey 1982, Cameron *et al.* 1983), Izu–Bonin fore-arc (Murton *et al.* 1992), Mariana trench and fore-arc (Hickey & Frey 1982), and northern termination of the Tonga trench (Falloon & Crawford 1991, Sobolev & Danyushevsky 1994), boninites from Troodos ophiolite (Cameron 1985, Bednarz & Schmincke 1994), and arc tholeiites from Kii Peninsula, southwestern Japan (Miyake 1985), Mariana, Yap and Palau trenches (Crawford *et al.* 1986, Beccaluva *et al.* 1986), New Caledonia (Cameron 1989), Bismarck arc (Basaltic Volcanism Study Project 1981, Johnson *et al.* 1985), New Hebrides arc (Dupuy *et al.* 1982), and Aleutians arc (Nye & Reid 1986). Chondrite C1 and N–MORB (open star) values are from Sun & McDonough (1989). Symbols are the same as on Figure 6.

With regard to the moderately incompatible elements, the batch melts produced from the NAMM mantle are fairly similar to liquids calculated to be in equilibrium with orthopyroxenite dykes (Figs. 8a, b). *HREE*, *MREE*, Zr, Hf, and Ti abundances in calculated liquids from type-I orthopyroxenites (except orthopyroxenite S3–O) and type-II orthopyroxenites S10–O and S11–O are roughly similar to those in melts produced by batch melting (≤10%) of depleted harzburgites in the NAMM suite, where no clinopyroxene melting is involved. This is consistent with the proposal that these orthopyroxenite-related melts were produced by batch melting of depleted NAMM harzburgites. On the other hand, the *REE*, Zr, Hf, and Ti abundances in liquids calculated from type-II orthopyroxenite S5–O and composite vein S5–CV are very similar to those in melts produced by batch melting (<20%) of depleted spinel lherzolites in the NAMM suite (Fig. 8b). Indeed, the participation of clinopyroxene during batch melting of these less-depleted sources give melts with higher and slightly less fractionated *HREE* abundances.

Reasoning the same way (and assuming that they are primary melts and not fractionation-related residua), magmas related to clinopyroxenitic and websteritic dykes, and to the type-I orthopyroxenite S3–O as well, could represent melts produced by second- to third-stage melting of residual mantle at shallow depth (<10 kbar), their sources being ultimately less depleted than those of the other NAMM orthopyroxenites. Indeed, the complete compositional range (but *LILE*) that exist among low-Ti subduction-related lavas, from boninites to island-arc basalts, may be explained (assuming they are primary melts) by the variable degree of depletion of their respective source (Fig. 8; Beccaluva & Serri 1988). The sources of boninites show variable degree of depletion, from clinopyroxene-free to clinopyroxene-bearing harzburgite compositions. The sources of boninites transitional to island-arc basalts presumably were derived from clinopyroxene-bearing harzburgite to clinopyroxene-poor depleted lherzolite compositions. In a same manner, we may argue that NAMM pyroxenite dykes crystallized from a spectrum of primary magma-types which represent batch melts (likely ≤10% of partial melting) of variously depleted residual mantle at shallow levels. This proposal would imply an earlier extraction of basaltic liquid. We may, thus, envisage a model whereby a residual diapir continued its adiabatic upwelling and eventually produced, at shallower levels and in the presence of a H_2O-rich fluid, successively more refractory and silica-rich melts, from boninitic–tholeiitic transitional melts (type-IV suite) to boninites (type-III suite) to extremely refractory boninitic melts (type-I and type-II suites). However, this scenario seems inconsistent with the general compositional trend of enrichment in a basaltic component that we observed upward in the apparent mantle section (from units 1d to 1b) among all NAMM pyroxenite intrusions taken together, and in particular among those from type-I to type-III suites. This inconsistency rather suggests that melts related to them were parental and underwent fractionation processes or others processes that acted to differentiate them during their migration.

Evolution of related magmas

There is a general trend of enrichment in Fe, Al, Ca, alkalis and incompatible trace-elements among intrusive pyroxenites, from deeper sites S9, S10 and S11 toward shallower sites, where intrusive pyroxenites typically show higher contents of Al, iron, alkalis and incompatible trace-elements, with less fractionated *MREE/HREE* values, and increased modal clinopyroxene. This, indeed, suggests that, parental or not, melts related to the NAMM pyroxenite dykes likely underwent a chemical evolution, leading to enrichment in the basaltic component during their upward migration in the upper mantle.

In terms of the composition of their minerals, and major-element and compatible trace-element concentrations, variations among type-I orthopyroxenites to type-III websterites are fairly consistent with a liquid line of descent controlled by the fractionation of olivine and minor spinel (Figs. 2, 3, 4 and 5). The progressive enrichment in *HREE* observed among melts related to these pyroxenites (Figs. 8a, c) also is roughly consistent with this interpretation, though this would imply very important percentages of crystallization. Melt compositions calculated from pyroxenites S7–O, S3–O and S4–W would represent residues from, respectively, 45, 70 and 80 wt.% (Yb) Rayleigh fractional crystallization of olivine ± spinel (99:1) [K_D values are from Bédard (1994)] from a parental melt composition calculated from orthopyroxenite S9–O. However, melt Cr and Ni contents calculated from type-I and type-III pyroxenites plotted against their melt Yb contents (Fig. 9) are only partly consistent with this interpretation; these melts form a general trend of increasing Yb content coupled with decreasing Cr and Ni contents, but this trend cannot be modeled by a Rayleigh fractional crystallization relationship, the Yb contents of melts being too high for given Cr and Ni contents. Moreover, calculated melts from type-I and type-III pyroxenites show variable Tb/Yb values, tending to increase as Yb increases, which is not compatible with a fractional crystallization relationship (Fig. 10).

In a general way, melts related to type-I orthopyroxenites show *MREE/HREE* values that are higher than those of melts produced by partial melting of NAMM harzburgites and lherzolites (Figs. 8, 10). Only melts related to type-II orthopyroxenites S10–O and S11–O show strongly fractionated *MREE* relative to *HREE*, and coupled extremely low Tb/Yb values and Yb contents, compatible with extremely depleted NAMM harzburgitic sources. Batch melts from more fertile sources, such as Balmuccia peridotites, which are interpreted to be residues after the separation of 4.5% MORB (Hartmann & Wedepohl 1993), will show coupled higher Tb/Yb values and Yb contents (Fig. 10). However, the fact that mineral compositions and major-element chemistry of type-I orthopyroxenites are more refractory than those of type-II orthopyroxenites is inconsistent with the hypothesis that they derived from a more fertile source (intermediate between NAMM and Balmuccia peridotites) than that of melts related to the type-II orthopyroxenites. Nevertheless, the similarity in their chemistries allows us to envisage a scenario whereby melts related to them derived from similarly depleted mantle sources, but other processes in addition to fractional crystallization acted to differentiate them.

A process that can lead to differential increases in *REE* abundances of migrating fractionating melts would involve assimilation of magnesian material from the host peridotitic wallrocks. Composite dykes S1–CV1, S1–CV2 and S5–CV systematically have intermediate mineral and whole-rock chemistries between those of dykes found at the same site and those of type-I orthopyroxenites. This evidence suggests to us that magma–mantle interactions indeed played a role in driving differentiation in the melts from which NAMM pyroxenites precipitated. Quick (1981), DePaolo (1981) and Kelemen and co-workers (Kelemen 1986, 1990, Kelemen *et al.* 1990, 1992) have pointed out that large variations in abundances of alkalis and more incompatible elements, combined with a very primitive major-element chemistry and nearly constant and high Mg-numbers, are a likely consequence of reaction between mantle-derived melts and host mantle. These reactions would principally be driven by chemical disequilibrium between intrusive melts and host peridotites, and may lead either to partial melting of the peridotite or to selective dissolution of minerals that are not stable in the intruding melt (Quick 1981, DePaolo 1981, Podvin *et al.* 1985, Kelemen 1986, 1990, Kelemen & Ghiorso 1986, Kelemen *et al.* 1990, 1992, Suhr & Robinson 1994). These reactions could also be enhanced by changes in pressure and temperature during the ascent of melts through the mantle peridotite (Fujii & Scarfe 1985, Hirose & Kushiro 1993).

The NAMM host peridotites that are in contact with intrusive pyroxenites show complex mineral, modal and chemical variations suggesting that continuous re-equilibration occurred between ascending melts and the surrounding peridotites of the NAMM ophiolitic mantle (Varfalvy *et al.* 1996). Intrusive magmas low in Al and Ca (type-I suite) could have depleted the surrounding peridotite in fusible elements by several mechanisms. The first of these involves dissolution–precipitation reactions and solid-solution exchange reactions between infiltrating melts and minerals from the wallrock. These exchanges produce residual chromite enriched in Cr, more magnesian orthopyroxene, and more diopsidic clinopyroxene. The fusible Ca–Al Tschermak component of clinopyroxene and the Al-component of spinel enter the melts. The second mechanism involves progressive selective dissolution of clinopyroxene from wallrocks as they react with clinopyroxene-undersaturated melts.

To illustrate the effects of assimilating clinopyroxene on fractionating melts related to the NAMM dykes, we generated a model liquid that undergoes coupled clinopyroxene assimilation from wallrocks and olivine ± spinel (99:1) fractionation, from an inferred melt related to type-I orthopyroxenite S9–O taken as starting point. The composition of assimilated clinopyroxene was calculated from the average composition of NAMM spinel lherzolites (unit 1e, Tables 5, 6) by mass-balance calculations. Equations for the assimilation–fractionation calculation are from DePaolo (1981). We assumed that the mass of the magma stays constant (mass crystallized = mass assimilated). Partition coefficients are from Bédard (1994), with the exception of the ${}^{ol}D_{Ni}$, which was assumed to be constant and equal to 10.

Assimilation of clinopyroxene by fractionating type-I-related melts would lead them to more rapid *HREE* enrichment relative to Cr and Ni depletions, caused by fractionation of olivine and minor spinel (Fig. 9), and more rapid enrichment in Tb compared to Yb (Fig. 10). Mantle clinopyroxene generally contains significant Ni and Cr, and assimilating them, concomitantly with olivine and spinel fractionation, may efficiently buffer reacting melts in these elements. In a similar way, assimilation of dissolved clinopyroxene from wallrock peridotites (until clinopyroxene saturation in the reacting melts is reached) may also be a major mechanism of buffering MgO, and SiO_2 as well, in olivine-fractionating melts, along with Mg–Fe solid–solution exchange reactions between wallrock minerals and reacting melts, as described by Kelemen (1990). The trend of increasing [Tb/Yb] as Yb contents increase among melts related to pyroxenites of the type-I suite to those of the type-III suite is quite consistent with coupled clinopyroxene assimilation and olivine ± spinel fractionation (Fig. 10). However, to reproduce the compositional evolution of melts from primitive type-I orthopyroxenites to type-III pyroxenites, large amounts of assimilated clinopyroxene are necessary (more than 80% of assimilated mass for Cr/Yb and Tb/Yb trends), eventually at higher rates of assimilation to reproduce the Ni/Yb evolution trend of these melts, which seems unrealistic.

Inversely, migrating tholeiitic melts may assimilate magnesian material from their hosting peridotitic wallrocks (Kelemen 1986, 1990). The occurrence of composite dykes that show a clinopyroxenitic core and orthopyroxenitic margins suggests that such a process occurred and may have driven differentiation in the melts from which NAMM pyroxenites precipitated. Composite dykes systematically have intermediate mineral and whole-rock chemistries between those of dykes found at the same site and those of the type-I orthopyroxenites, and melts related to the more primitive members of the type-I suite are roughly consistent with melts produced by batch melting (≤10%) of surrounding harzburgites. We thus simplified the process of assimilation of magnesian material from the host mantle by a migrating clinopyroxenite-related melt, by simple binary mixing between melt in equilibrium with type-IV clinopyroxenite S1–C1 and a liquid produced by 10% partial melting of average NAMM depleted spinel harzburgite from unit 1d. Figure 10 shows that, in terms of *HREE* abundances, a continuous compositional trend exists among melts related to pyroxenites of the type-I suite toward those of the type-IV suite, which is remarkably consistent with the calculated mixing trend between ultra-depleted and S2–C1 clinopyroxenite-related magmas. According to this model, with regard to *HREE* abundances, type-IV clinopyroxenite S1–C2 and composite vein S1–CV1 would result from the addition of ~45–50% of a melt fraction produced by 10% partial melting of NAMM depleted spinel harzburgites to S1–C2 clinopyroxenite-related melt, whereas type-I orthopyroxenites from S9–O to S6–O would result from the addition of ~1 to 10% S1–C1 clinopyroxenite-related melt component to melts produced by 10% partial melting of NAMM harzburgites.

Melts related to type-I orthopyroxenite S3–O and type-III websterite plot slightly apart, having higher Yb-contents for a given [Tb/Yb] value. It is possible that these melts derived from such a mixture (~10% S1–C1 clinopyroxenite-related melt) but underwent a more rapid enrichment in Yb from combined assimilation and fractionation processes. Cr variations in these melts (Fig. 9a), and in other type-I and type-IV melts, indeed suggest that fractionation of chromian spinel occurs, possibly combined with clinopyroxene assimilation, which will lead to Cr buffering of reacting melts and their rapid enrichment in the *HREE*. Ni variations in type-I and type-III-related melts suggest that olivine fractionation also occurs (Fig. 9b), which is consistent with inferences made from mineral and major-element chemistries. Melts related to type-I orthopyroxenite S3–O and type-III websterite also plot slightly apart, being too rich in Ni for a given Yb abundance to simply have been derived from other type-I melts by a fractionation process. This discrepancy suggests that these melts also underwent Ni buffering and a more rapid enrichment in Yb by assimilating clinopyroxene from wallrocks. The fact that no decrease (composite vein S1–CV1) or increase (clinopyroxenite S1–C2 and composite vein S5–CV) in Ni contents relative to the mixing trend is observed in some NAMM pyroxenite-related melts suggests that olivine fractionation does not always occur during the evolution of NAMM melts. Increases in their Ni contents may be satisfactorily explained by assimilation of clinopyroxene from the wallrocks. It is also possible that these melts assimilated, along with other magnesian material from wallrocks, significant amounts of Fe–Ni sulfide phases. The fact that these dykes also show high MgO and SiO_2 contents is consistent with the proposal that they underwent such magma–mantle interactions.

The compositional trend formed by type-IV clinopyroxenite S1–C1, type-II orthopyroxenite S5–O, type-II orthopyroxenites S10–O and S11–O to the proposed primitive parental melt of type-I to type-III orthopyroxenites (low fractions of batch melts of ultra-depleted harzburgites) is roughly compatible with increasing partial melting of mantle peridotite. However, the fact that these "primary" melts show large variations in abundances of alkalis, Al and incompatible elements, combined with a very primitive major-element chemistry, and nearly constant and high Mg-numbers and Ni contents, is a likely consequence of reaction between variously depleted mantle-derived melts and surrounding peridotites.

We may, thus, envisage a model whereby NAMM pyroxenites have not directly crystallized from primary magmas generated by the melting of ultra-depleted mantle. Rather, the magmas related to them acquired the signatures of such mantle by reacting and reaching equilibrium with large volumes of variously depleted peridotites at shallower levels during their migration through the mantle. This proposal would also imply earlier episode(s) of extensive extraction of basalts, producing extremely depleted harzburgite and lherzolite residues. The NAMM pyroxenite dykes may have formed during a final magmatic event, in which a residual diapir continued its adiabatic upwelling and eventually produced, at shallower levels, in the presence of H_2O-rich fluids, depleted magnesium-rich tholeiitic melts that fractionated and re-equilibrated with variously depleted residual mantle during their ascent throughout the mantle. We propose that the variety of compositions among melts related to NAMM pyroxenites resulted from fractional crystallization of olivine ± spinel, assimilation of dissolved clinopyroxene from wallrocks, and magma mixing, in various proportions, between a primary low-Ti magnesian tholeiitic component and low fractions of melts produced by partial re-melting of surrounding harzburgites or lherzolites.

Origin of the LILE enrichment

The model proposed to explain the trace-element signatures observed in NAMM pyroxenite dykes cannot satisfactorily account for the *LILE* and local *LREE* enrichment of these dykes. Orthopyroxenitic and composite dykes typically show a more important *LILE* enrichment, which is compatible with the proposal that they represent melts that assimilated harzburgitic material (NAMM harzburgites being enriched in *LILE*); however, type-I and type-II orthopyroxenites show *LILE* enrichment that is greater than that of melts produced by partial melting of NAMM harzburgites (Fig. 8).

Depleted harzburgites in the NAMM suite exhibit *LILE*- and *LREE*-enriched, concave-upward normalized trace-element patterns. Such patterns are generally attributed to post-melting enrichment processes caused by porous flow of low melt-fractions or H_2O- or CO_2-rich fluids (Wilshire *et al.* 1980, Wilshire1984, 1987, Navon & Stolper 1987, McDonough & Frey 1989, Fabriès *et al.* 1989, Bodinier *et al.* 1990, Vasseur *et al.* 1991, Takazawa *et al.* 1992, Parkinson *et al.* 1992, Van der Wal & Bodinier 1996). It is possible that a widespread *LILE–LREE* component of the NAMM mantle was preferentially incorporated into the low melt-fractions (≤10%), so that the mantle we see now is the residue from this event, not its source. Thus, the high *LILE* and *LREE* abundances in the dyke melts would represent pre-melting conditions of the source. The fact that NAMM orthopyroxenite dykes that likely equilibrated with harzburgites contain, like them, an important *LREE* enrichment, whereas those that likely equilibrated with lherzolites (not *LREE*-enriched) do not, is consistent with this proposal. Alternatively, it is possible that addition of a mobile *LILE*- and *LREE*-enriched fluid component passing through the depleted NAMM mantle occurred during the NAMM dyke emplacement, and superimposed on their *LILE* and *LREE* signatures.

Conclusions and Tectonic Implications

Pyroxenitic intrusions in the NAMM suite are characterized by high Mg-numbers, high Ni and Cr contents, variable Ca contents, low Al and alkalis contents, and strongly depleted *MREE*, *HREE*, Ta, Zr, Hf and Ti abundances, with relative *LILE* enrichments (with or without *LREE* enrichments). The early precipitation of orthopyroxene, inferred by textural observations and compositional variations, seems to imply that the liquids from which they precipitated were saturated to oversaturated in silica, and likely had a SiO_2 content typical of andesites. On the basis of their major- and transition-element contents, NAMM pyroxenites can be grouped into four suites: a type-I low-Al orthopyroxenite suite, a type-II orthopyroxenite suite that is more Al-rich, a type-III websterite suite, and a type-IV high-Al clinopyroxenite suite. The more evolved members of the type-I and -III suites show decreased Mg, Cr and Ni contents with increased concentrations of Fe, Ca, Al, alkalis, Ti, Sc, V and incompatible trace elements. Part of this variation could result from initial fractionation of olivine and minor chromian spinel. The striking enrichment in incompatible elements, coupled with weakly decreasing Mg, Cr and Ni seen in some members, could reflect (in addition to fractional crystallization) interactions with rocks of the upper mantle involving assimilation of clinopyroxene from peridotite wallrocks. Melts from which type-IV clinopyroxenites crystallized resemble modern magnesian quartz-normative tholeiites found in the Mariana fore-arc, and which are interpreted to have formed during second-stage melting of residual mantle at shallow levels (*e.g.*, Duncan & Green 1987). Our data suggest that NAMM pyroxenites have not crystallized from primary magmas generated by the melting of ultra-depleted mantle, but rather acquired the signatures of such mantle by reacting and reaching equilibrium with large volumes of variously depleted peridotites at shallower levels during their migration through the mantle, involving assimilation of low melt-fractions (≤10%) of metasomatized depleted peridotite wallrocks into migrating tholeiitic melts.

The magmatic and tectonic affinity of magmas in the Bay of Islands ophiolitic complex (BOI) is the subject of an ongoing debate. Early petrological and geochemical studies showed that whereas mafic pillow lavas and diabases of the BOI have major- and trace-element compositions and depleted *LREE* patterns similar to MORB, the data could not discriminate between a true mid-ocean ridge environment and a supra-subduction spreading environment (Williams & Malpas 1972, Suen *et al.* 1979). On the basis of high Cr/Al values in the chromian spinel, Dick & Bullen (1984) suggested that some Bay of Islands ophiolite cumulates had a subduction-zone affinity. Conversely, Casey *et al.* (1985) and Siroky *et al.* (1985) showed that basalts and diabases from the Bay of Islands ophiolites are very similar to MORB. They argued for a normal ridge environment. More recent petrological and chemical data on cumulates of the lower crust (Bédard 1991, Bédard *et al.* 1994, Bédard & Hébert 1996) show clear arc or boninitic signatures [abundant orthopyroxene, low-Ti pyroxenes, high-(Cr/Al) spinel, *LILE*-enriched trace-element profiles]. Recent geochemical and isotopic data on BOI basalts and trondhjemites reveal negative Nb–Ta anomalies, considered characteristic of arc suites (Jenner *et al.* 1991, Elthon 1991). Evidence of subduction-related melts is also present in the mantle section of the BOI (Edwards 1990, 1991, 1995, Edwards & Malpas 1995).

The composition and evolution of NAMM intramantle pyroxenite dykes are very similar to those seen in modern magnesian andesites and boninites from the western Pacific. If the analogy holds true, then we may infer that primitive boninitic melts underwent similar interactions with depleted mantle, and acquired their unusual signature by reacting and reaching equilibrium with large volumes of variously depleted peridotites at shallower levels during their migration through the mantle. A fore-arc environment appears to have the combination of factors needed to generate boninitic magmas: high thermal gradients, shallow depths, high activities of H_2O and limited melting of metasomatized ultra-depleted mantle sources in a tensional environment. This would imply that the North Arm Mountain ophiolitic massif passed through a fore-arc environment at a late stage in its history, immediately prior to its obduction onto the North American margin.

ACKNOWLEDGEMENTS

Funding was provided by the Natural Sciences and Engineering Research Council of Canada (NSERC) and by the Fonds pour la Formation de Chercheurs et l'Aide à la Recherche (FCAR). We are grateful to G. Suhr, R.F. Martin, G.T Nixon, J. Malpas and an anonymous referee for their constructive comments of the manuscript, and to INRS-Géoressources (Complexe Géoscientifique de Québec) and the Geological Survey of Canada for the logistical facilities.

REFERENCES

ALLÈGRE, C.J. & MINSTER, J.F. (1978): Quantitative models of trace element behavior in magmatic processes. *Earth Planet. Sci. Lett.* **38**, 1-25.

ARCHIBALD, D.A. & FARRAR, E. (1976): K–Ar ages of amphiboles from the Bay of Islands ophiolite and Little Port Complex, western Newfoundland, and their geological implications. *Can. J. Earth Sci.* **13**, 520-529.

BASALTIC VOLCANISM STUDY PROJECT (1981): *Basaltic Volcanism on the Terrestrial Planets.* Pergamon Press Inc., New York, N.Y.

BECCALUVA, L. & SERRI, G. (1988): Boninitic and low-Ti subduction-related lavas from intraoceanic arc-backarc systems and low-Ti ophiolites: a reappraisal of their petrogenesis and original tectonic setting. *Tectonophys.* **146**, 291-315.

________, ________ & DOSTAL, J. (1986): Geochemistry of volcanic rocks from the Mariana, Yap and Palau trenches bearing on the tectono-magmatic evolution or the Mariana trench – arc – backarc system. *In* The Origin of Arcs (F.C. Wezel, ed.). Elsevier, Amsterdam, The Netherlands (481-508).

BÉDARD, J.H. (1991): Cumulate recycling and crustal evolution in the Bay of islands ophiolite. *J. Geol.* **99**, 225-249.

________ (1994): A procedure for calculating the equilibrium distribution of trace elements among the minerals of cumulate rocks, and the concentration of trace elements in the coexisting liquids. *Chem. Geol.* **118**, 143-153.

________ & HÉBERT, R. (1996): The lower crust of the Bay of Islands ophiolite, Canada: petrology, mineralogy, and the importance of syntexis in magmatic differentiation in ophiolites and at ocean ridges. *J. Geophys. Res.* **101**, 25105-25124.

________, ________, VARFALVY, V. & MÉLANÇON, B. (1994): Boninite magmatism in the Bay of Islands ophiolite. *Trans. Am. Geophys. Union* (*Eos*) **75**, 731 (abstr.).

BEDNARZ, U. & SCHMINCKE, H.-U. (1994): Petrological and chemical evolution of the northeastern Troodos extrusive series, Cyprus. *J. Petrol.* **35**, 489-523.

BENCE, A.E. & ALBEE, A.L. (1968): Empirical correction factor for electron microanalysis of silicates and oxides. *J. Geol.* **76**, 382-403.

BERCLAZ, A., BÉDARD, J.H., HÉBERT, R., VARFALVY, V., MÉLANÇON, B., YAO, K.R. & EL BILABI, L. (1994): Tectonic evolution of the plutonic section of the Bay of Islands ophiolite. *Trans. Am. Geophys. Union* (*Eos*) **75**, 650-651 (abstr.).

BLOOMER, S.H. & HAWKINS, J.W. (1987): Petrology and geochemistry of boninite series volcanic rocks from the Mariana trench. *Contrib. Mineral. Petrol.* **97**, 361-377.

BODINIER, J.-L., FABRIÈS, J., LORAND, J.-P., DOSTAL, J. & DUPUY, C. (1987): Geochemistry of amphibole pyroxenite veins from the Lherz and Freychinède ultramafic bodies (Ariège, French Pyrenées). *Bull. Minéral.* **110**, 345-358.

________, VASSEUR, G., VERNIÈRES, J., DUPUY, C. & FABRIÈS, J. (1990): Mechanisms of mantle metasomatism: geochemical evidence from the Lherz orogenic peridotite. *J. Petrol.* **31**, 597-628.

BOYD, F.R. (1959): Hydrothermal investigations of amphiboles. *In* Researches in Geochemistry **1** (P.H. Abelson, ed.). John Wiley and Sons, New York, N.Y. (377-396).

BUDAHN, J.R. (1986): Evidence for equilibrium conditions during the partitioning of nickel between olivine and komatiite liquids. *Am. Mineral.* **71**, 1337-1342.

CAMERON, W.E. (1985): Petrology and origin of primitive lavas from the Troodos ophiolite, Cyprus. *Contrib. Mineral. Petrol.* **89**, 239-255.

________ (1989): Contrasting boninite–tholeiite associations from New Caledonia. *In* Boninites (A.J. Crawford, ed.). Unwin Hyman, London, U.K. (314-338).

________, MCCULLOCH, M.T. & WALKER, D.A. (1983): Boninite petrogenesis: chemical and Nd–Sr isotopic constraints. *Earth Planet. Sci. Lett.* **65**, 75-89.

________, NISBET, E.G. & DIETRICH, V.J. (1979): Boninites, komatiites and ophiolitic basalts. *Nature* **280**, 550-553.

CASEY, J.F., DEWEY, J.F., FOX, P.J., KARSON, J.A. & ROSENCRANTZ, E. (1981): Heterogeneous nature of the oceanic crust and upper mantle: a perspective from the Bay of Islands ophiolite complex. *In* The Sea **7** (C. Emiliani, ed.). John Wiley and Sons, New York, N.Y. (305-338).

________, ELTHON, D.L., SIROKY, F.X., KARSON, J.A. & SULLIVAN, J. (1985): Geochemical and geological evidence bearing on the origin of the Bay of Islands and Coastal Complex ophiolites of western Newfoundland. *Tectonophys.* **116**, 1-40.

CAWOOD, P.A. & SUHR, G. (1992): Generation and obduction of ophiolites: constraints from the Bay of Islands Complex, western Newfoundland. *Tectonics.* **11**, 884-897.

________, WILLIAMS, H., O'BRIEN, S.J. & O'NEIL, P.P. (1988): A geologic cross-section of the Appalachian Orogen. *Geol. Assoc. Can., Field Excursion Guidebook.*

CRAWFORD, A.J., BECCALUVA, L., SERRI, G. & DOSTAL, J. (1986): Petrology, geochemistry and tectonic implications of volcanics dredged from the intersection of the Yap and Mariana trenches. *Earth Planet. Sci. Lett.* **80**, 265-280.

________, FALLOON, T.J. & GREEN, D.H. (1990): Classification, petrogenesis and tectonic setting of boninites. *In* Boninites (A.J. Crawford, ed.). Unwin Hyman, London, U.K. (1-49).

DALLMEYER, R.D. & WILLIAMS, H. (1975): ^{40}Ar/^{39}Ar ages for the Bay of Islands metamorphic aureole: their bearing on the timing of Ordovician ophiolite obduction. *Can. J. Earth Sci.* **12**, 1685-1690.

DEPAOLO, D.J. (1981): Trace element and isotopic effects combined wallrock assimilation and fractional crystallization. *Earth Planet. Sci. Lett.* **53**, 189-202.

DICK, H.J.B. (1977): Partial melting in the Josephine peridotite. I. The effect on mineral composition and its consequence for geobarometry and geothermometry. *Am. J. Sci.* **277**, 801-832.

________ (1989): Abyssal peridotites, very low spreading ridges and ocean ridge magmatism. *In* Magmatism in the Ocean Basins (A.D. Saunders & M.J. Norry, eds.). *Geol. Soc., Spec. Publ.* **42**, 71-105.

________ & BULLEN, T. (1984): Chromian spinel as a petrogenetic indicator in abyssal and alpine-type peridotites and spacially associated lavas. *Contrib. Mineral. Petrol.* **86**, 54-76.

________ & FISHER, R.L. (1984): Mineralogic studies of the residues of mantle melting: abyssal and alpine-type peridotites. *In* Kimberlite II – The mantle and crust–mantle relationships (J. Kornprobst, ed.). Elsevier, Amsterdam, The Netherlands (295-308).

DUNCAN, R.A. & GREEN, D.H. (1987): The genesis of refractory melt in the formation of oceanic crust. *Contrib. Mineral. Petrol.* **96**, 326-342.

DUPUY, C., DOSTAL, J., MARCELOT, G., BOUGAULT, H., JORON, J.L. & TREUIL, M. (1982): Geochemistry of basalts from central and southern New Hebrides arc: implication for their source rock composition. *Earth Planet. Sci. Lett.* **60**, 207-225.

EDWARDS, S.J. (1990): Harzburgite and refractory melts in the Lewis Hills massif, Bay of Islands ophiolite complex: the base-metals and precious-metals story. *Can. Mineral.* **28**, 537-552.

________ (1991): *Magmatic and Fluid Processes in the Upper Mantle: a Study of the Bay of Islands Ophiolite Complex, Newfoundland.* Ph.D. thesis, Memorial Univ. of Newfoundland, St. John's, Newfoundland.

________ (1995): Boninitic and tholeiitic dykes in the Lewis Hills mantle section of the Bay of Islands ophiolite: implication for magmatism adjacent to a fracture zone in a back-arc spreading environment. *Can. J. Earth Sci.* **32**, 2128-2146.

________ & MALPAS, J. (1995): Multiple origins for mantle harzburgites: examples from the Lewis Hills, Bay of Islands ophiolite, Newfoundland. *Can. J. Earth Sci.* **32**, 1046-1057.

ELTHON, D. (1991): Geochemical evidences for the formation of the Bay of Islands ophiolite above a subduction zone. *Nature* **354**, 140-143.

________ & SCARFE, C.M. (1984): High-pressure phase equilibria of a high-magnesia basalt and the genesis of primary oceanic basalts. *Am. Mineral.* **69**, 1-15.

FABRIÈS, J., BODINIER, J.-L., DUPUY, C., LORAND, J.-P. & BENKERROU, C. (1989): Evidence for modal metasomatism in the orogenic spinel lherzolite body from Caussou (northeastern Pyrenees, France). *J. Petrol.* **30**, 199-228.

FALLOON, T.J. & CRAWFORD, A.J. (1991): The petrogenesis of high-calcium boninite lavas dredged from the northern Tonga ridge. *Earth Planet. Sci. Lett.* **102**, 375-394.

________, GREEN, D.H. & MCCULLOCH, M.T. (1989): Petrogenesis of high-Mg and associated lavas from the north Tonga Trench *In* Boninites (A.J. Crawford, ed.). Unwin Hyman, London, U.K. (357-395).

FREY, F.A., SUEN, C.J. & STOCKMAN, H.W. (1985): The Ronda high temperature peridotite: geochemistry and petrogenesis. *Geochim. Cosmochim. Acta* **49**, 2469-2491.

FUJII, T. & SCARFE, C.M. (1985): Composition of liquids coexisting with spinel lherzolite at 10 kbar and the genesis of MORBs. *Contrib. Mineral. Petrol.* **90**, 18-28.

GARRIDO, C.J. (1995): *Estudio geoquímico de las capas máficas del macizo ultramáfico de Ronda (Cordillera Bética, España).* Ph.D. thesis, Univ. of Granada, Granada, Spain.

________ & VAN DER WAL, D. (1995): Structural petrology and geochemistry of the Ronda ultramafic massif: field trip to the Ronda massif. *In* Doc., Second Int. Workshop on Orogenic Lherzolites and Mantle Processes **2** (H.G. Barsczus & F. Gervilla, eds.). CSIC – University of Granada, Granada, Spain.

GILL, J.B. (1976): Composition and the age of Lau Basin and Ridge volcanic rocks: implications for evolution of an interarc basin and remnant arc. *Geol. Soc. Am., Bull.* **87**, 1384-1395.

GREEN, D.H. (1973): Experimental melting studies on a model upper mantle composition at high pressure under water-saturated and water-unsaturated conditions. *Earth Planet. Sci. Lett.* **19**, 37-53.

HAMLYN, P.R. & BONATTI, E. (1980): Petrology of mantle-derived ultramafics from the Owen fracture zone, North-west Indian Ocean: implications for the nature of the oceanic upper mantle. *Earth Planet. Sci. Lett.* **48**, 65-79.

Hartmann, G. & Wedepohl, K.H. (1993): The composition of peridotite tectonites from the Ivrea Complex, Northern Italy: residues from melt extraction. *Geochim. Cosmochim. Acta* **57**, 1761-1782.

Hawkins, J.W., Jr. (1977): Petrologic and geochemical charateristics of marginal basin basalts. *In* Island Arc, Deep Sea Trenches and Back-Arc Basins (third edition; M. Talwani & W.C. Pitman, III, eds.). *Am. Geophys. Union, Maurice Ewing Ser.* **1**, 355-365.

________ (1980): Petrology of back-arc basins and island arcs: their possible roles in the origin of ophiolites. *In* Proc. Int. Ophiolite Symp. (A. Panayiotou, ed.). Ministry Dep. of Agriculture and Natural Resources, Geological Survey, Nicosia, Cyprus (244-254).

________ & Melchior, J.T. (1985): Petrology of Mariana trough and Lau basin basalts. *J. Geophys. Res.* **90**, 11431-11468.

Hébert, R., Varfalvy, V., Bédard, J.H., Berclas, A. (1996): The transition from upper mantle to lower crust in the North Arm Mountain Massif, Bay of Islands ophiolite, Newfoundland, Canada. *Int. Geol. Congress, 30th Meet., Abstr. Vol.*, 26.

Hickey, R.L. & Frey, F.A. (1982): Geochemical characteristics of boninite series volcanics: implications for their source. *Geochim. Cosmochim. Acta* **46**, 2099-2115.

Hirose, K. & Kushiro, I. (1993): Partial melting of dry peridotites at high pressures: determination of compositions of melts segregated from peridotite using aggregates of diamond. *Earth Planet. Sci. Lett.* **114**, 477-489.

Irvine, T.N. & Findlay, T.C. (1972): Alpine-type peridotite with particular reference to the Bay of Islands igneous complex. *Can. Dep. Energy, Mines and Resources, Spec. Publ.* **42**, 77-128.

Jamieson, R.A. (1986): P–T path from high temperature shear zones beneath ophiolites. *J. Metamorphic Geol.* **4**, 3-22.

Jenkins, D.M. (1983): Stability and composition relations of calcic amphiboles in ultramafic rocks. *Contrib. Mineral. Petrol.* **83**, 375-384.

Jenner, G.A. (1981): Geochemistry of high-Mg andesites from Cape Vogel, Papua New Guinea. *Chem. Geol.* **33**, 307-332.

________, Dunning, G.R., Malpas, J., Brown, M. & Brace, T. (1991): Bay of Islands and Litle Port complexes, revisited: age, geochemical and isotopic evidence confirm supra-subduction zone origin. *Can. J. Earth Sci.* **28**, 1635-1652.

Johnson, R.W., Jaques, A.L., Hickey, R.L., McKee, C.O. & Chappell, B.W. (1985): Manam Island, Papua New Guinea: petrology and geochemistry of a low-TiO_2 basaltic island-arc volcano. *J. Petrol.* **26**, 283-323.

Kelemen, P.B. (1986): Assimilation of ultramafic rock in subduction-related magmatic arcs. *J. Geol.* **94**, 829-843.

________ (1990): Reaction between ultramafic rock and fractionating basaltic magma. I. Phase relations, the origin of calc-alkaline magma series, and the formation of discordant dunite. *J. Petrol.* **31**, 51-98.

________, Dick, H.J.B. & Quick, J.E. (1992): Formation of harzburgite by pervasive melt/rock reaction in the upper mantle. *Nature* **358**, 635-641.

________ & Ghiorso, M.S. (1986): Assimilation of peridotite in zoned calc-alkaline plutonic complexes: evidence from the Big Jim complex, Washington Cascades. *Contrib. Mineral. Petrol.* **94**, 12-28.

________, Johnson, K.T.M., Kinzler, R.T. & Irving, A.J. (1990): High-field-strength element depletions in arc basalts due to mantle–magma interaction. *Nature* **345**, 521-524.

Kinzler, R.J. & Grove, T.L. (1992): Primary magmas of Mid-Ocean Ridge basalts. 1. Experiments and methods. *J. Geophys. Res.* **97**, 6885-6906.

Kostopoulos, D.K. (1991): Melting of the shallow upper mantle: a new perspective. *J. Petrol.* **32**, 671-699.

Kuroda, N., Shiraki, K. & Urano, H. (1978): Boninite as possible calc-alkalic primary magma. *Bull. Volcanol.* **41**, 563-575.

Kushiro, I. (1969): The system forsterite – diopside – silica with and without water at high pressures. *Am. J. Sci.* **267**-A, 269-294.

________, Syono, Y. & Akimoto, S. (1968): Melting of a peridotite nodule at high pressures and high water pressures. *J. Geophys. Res.* **73**, 6023-6029.

Laurent, R. & Kacira, N. (1987): Chromite deposits in the Appalachian ophiolites. *In* Evolution of Chromium Ore Fields (W.C. Stowe, ed.). Van Nostrand Reinhold Co., New York, N.Y. (169-193).

Malpas, J.G. (1976): *The Petrology and Petrogenesis of the Bay of Islands Ophiolite Suite, Western Newfoundland.* Ph.D. thesis, Memorial Univ. of Newfoundland, St. John's, Newfoundland.

McDonough, W.F. & Frey, F.A. (1989): Rare earth element in upper mantle rocks. *In* Geochemistry and Mineralogy of Rare Earth Elements (B.R. Lipin & G.A. McKay, eds.). *Rev. Mineral.* **21**, 99-145.

Mercier, J.-C.C. (1980) Single-pyroxene thermobarometry. *Tectonophys.* **70**, 1-37.

Michael, P.J. & Bonatti, E. (1985): Peridotite composition from the North Atlantic: regional and tectonic variations and implication for partial melting. *Earth Planet. Sci. Lett.* **73**, 91-104.

MIYAKE, Y. (1985): MORB-like tholeiites formed within the Miocene forearc basin, southwest Japan. *Lithos* **18**, 23-34.

MORSE, S.A. (1980): *Basalt and Phase Diagrams.* Springer-Verlag, Heidelberg, Germany.

MURTON, J.B., PEATE, D.W., ARCULUS, R.J., PEARCE, J.A. & VAN DER LAAN, S. (1992): Trace-element geochemistry of volcanic rocks from site 786: the Izu–Bonin forearc. *In* Proc. Ocean Drilling Program, Scientific Results **125** (P. Fryer, J.A. Pearce, L.B. Stokking *et al.*, eds.). Ocean Drilling Program, College Station, Texas (211-235).

NAVON, O. & STOLPER, E. (1987): Geochemical consequences of melt percolation: the upper mantle as a chromatographic column. *J. Geol.* **95**, 285-307.

NYE, C.J. & REID, M.R. (1986): Geochemistry of primary and least fractionated lavas from Okmok volcano, central Aleutians: implications for arc magma genesis. *J. Geophys. Res.* **91**, 10271-10287.

O'HARA, M.J. (1968): The bearing of phase equilibria studies in synthetic and natural systems on the origin and evolution of basic and ultrabasic rocks. *Earth Sci. Rev.* **4**, 69-133.

PARKINSON, I.J., PEARCE, J.A., THIRLWALL, M.F., JOHNSON, K.T.M. & INGRAM, G. (1992): Trace-element geochemistry of peridotites from the Izu–Bonin–Mariana forearc, Leg 125. *In* Proc. Ocean Drilling Program, Scientific Results **125** (P. Fryer, J.A. Pearce, L.B. Stokking *et al.*, eds.). Ocean Drilling Program, College Station, Texas (487-506).

PEARCE, J.A. (1982): Trace element characteristics of lavas from destructive plate boundaries. *In* Andesites (R.S. Thorpe ed.). John Wiley and Sons, London, U.K. (525-548).

PODVIN, P., BERGER, E.T. & VANNIER, M. (1985): Interactions géochimiques liées à la mise en place de dikes pyroxénitiques et gabbroïques dans des harzburgites ophiolitiques: exemple du Massif de Humboldt (Nouvelle-Calédonie). *Bull. Minéral.* **108**, 45-62.

QUICK, J.E. (1981): The origin and signifiance of large, tabular dunite bodies in the Trinity peridotite, northern California. *Contrib. Mineral. Petrol.* **78**, 413-422.

REUBER, I., WHITECHURCH, H. & JUTEAU, T. (1985): Successive generations of coarse grained dykelets in the ophiolite complex of Antalya, Turkey: products of partial fusion and residual liquides. *Ofioliti* **10**, 35-62.

RICCIO, L. (1976): *Stratigraphy and Petrology of the Peridotite–Gabbro Component of the Western Newfoundland Ophiolites.* Ph.D. thesis, Univ. of Western Ontario, London, Ontario.

ROEDER, P.L. & EMSLIE, R.F. (1970): Olivine–liquid equilibrium. *Contrib. Mineral. Petrol.* **29**, 275-289.

SINTON, J.M. & DETRICK, R.S. (1992): Mid-ocean ridge magma chambers. *J. Geophys. Res.* **97**, 197-216.

SIROKY, F.X., ELTHON, D.L., CASEY, J.F. & BUTLER, J.C. (1985): Major element variations in basalts and diabases from the North Arm Mountain massif, Bay of Islands ophiolite: implications for magma chamber processes at mid-ocean ridges. *Tectonophys.* **116**, 41-61.

SMITH, C.H. (1958): Bay of Islands igneous complex, western Newfoundland. *Geol. Surv. Can., Mem.* **290**.

SMITH, S.E. & ELTHON, D. (1988): Mineral compositions of plutonic rocks from the Lewis Hills massif, Bay of Islands ophiolite. *J. Geophys. Res.* **93**, 3450-3468.

SOBOLEV, A.V. & DANYUSHEVSKY, L.V. (1994): Petrology and geochemistry of boninites from the north termination of the Tonga trench: constraints on the generation conditions of primary high-Ca boninite magmas. *J. Petrol.* **35**, 1183-1211.

SUEN, C.J. & FREY, F.A. (1987): Origins or the mafic and ultramafic rocks in the Ronda peridotite. *Earth Planet. Sci. Lett.* **85**, 183-202.

________, ________ & MALPAS, J. (1979): Bay of Islands ophiolite suite, Newfoundland: petrologic and geochimical characteristics with emphasis on rare earth element geochemistry. *Earth Planet. Sci. Lett.* **45**, 337-348.

SUHR, G. & ROBINSON, P.T. (1994): Origin of mineral chemical stratification in the mantle section of the Table Mountain massif (Bay of Islands Ophiolite, Newfoundland, Canada). *Lithos* **31**, 81-102.

SUN, SHEN-SU & MCDONOUGH, W.F. (1989): Chemical and isotopic systematics of oceanic basalts: implications for the mantle composition and processes. *In* Magmatism in the Ocean Basins (A.D. Saunders & M.J. Norry, eds.). *Geol. Soc., Spec. Publ.* **42**, 313-345.

TAKAHASHI, N. (1992): Evidence for melt segregation towards fractures in the Horoman mantle peridotite complex. *Nature* **359**, 52-55.

TAKAZAWA, E., FREY, F.A., SHIMIZU, N., OBATA, M. & BODINIER, J.-L. (1992): Geochemical evidence for melt migration and reaction in the upper mantle. *Nature* **359**, 55-58.

TATSUMI, Y. & ISHIZAKA, K. (1982): Origin of high-magnesian andesites in the Setouchi volcanic belt, southwest Japan. I. Petrographical and chemical characteristics. *Earth Planet. Sci. Lett.* **60**, 293-304.

TAYLOR, R.N., NESBITT, R.W., VIDAL, P., HARMON, R.S., AUVRAY, B. & CROUDACE, I.W. (1994): Mineralogy, chemistry, and genesis of the boninite series volcanics, Chichijima, Bonin Islands, Japan. *J. Petrol.* **35**, 577-617.

UMINO, S. (1985): Volcanic geology of Chichijima, the Bonin Islands (Ogasawara Islands). *J. Geol. Soc. Japan* **91**, 505-523.

________ (1986): *Geological and Petrological Study of Boninites and Related Rocks from Chichijima, Bonin Islands.* Ph.D. thesis, Univ. of Tokyo, Tokyo, Japan.

VAN DER LANN, S.R., ARCULUS, R.J., PEARCE, J.A. & MURTON, B.J. (1992): Petrography, mineral chemistry, and phase relations or the basement boninite series of site 786, Izu–Bonin forearc. *In* Proc. Ocean Drilling Program, Scientific Results **125** (P. Fryer, J.A. Pearce, L.B. Stokking *et al.*, eds.). Ocean Drilling Program, College Station, Texas (171-201).

VAN DER WAL, D. & BODINIER, J.-L. (1996): Origin of the recrystallisation front in the Ronda peridotite by km-scale pervasive porous melt flow. *Contrib. Mineral. Petrol.* **122**, 387-405.

VARFALVY, V. (1994): *Interactions magma–manteau dans les péridotites du massif ophiolitique de North Arm, Bay of Islands, Terre-Neuve.* Mémoire M.Sc., Univ. Laval, Sainte-Foy, Québec.

________, HÉBERT, R. & BÉDARD, J.H. (1996): Interactions between melt and upper-mantle peridotite in the North Arm Mountain massif, Bay of Islands ophiolite, Newfoundland, Canada: implications for the genesis of boninitic and related magmas. *Chem. Geol.* **129**, 71-90.

________, ________, ________ & LAFLÈCHE, M.R. (1995): Petrological and geochemical evidences of melt migration and interaction with upper mantle rocks in the North Arm Mountain massif, Bay of Islands, Newfoundland, Canada: implications for the genesis of boninitic magmas. *In* Doc. Second Int. Workshop on Orogenic Lherzolites and Mantle Processes **1** (H.G. Barsczus & F. Gervilla, eds.). CSIC – University of Granada, Granada, Spain (73-74).

VASSEUR, G., VERNIÈRES, J. & BODINIER, J.-L. (1991): Modelling of trace element transfer between mantle melt and heterogranular peridotite matrix. In Orogenic Lherzolites and Mantle Processes (M.A. Menzies, C. Dupuy & A. Nicolas, eds.). *J. Petrol., Spec. Vol.*, 41-54.

WALKER, D.A. & CAMERON, W.E. (1983): Boninite primary magmas: Evidence from the Cape Vogel Peninsula, PNG. *Contrib. Mineral. Petrol.* **83**, 150-158.

WILLIAMS, H. (1973): Bay of Islands map-area, Newfoundland. *Geol. Surv. Can., Pap.* **72-34**.

________ (1979): The Appalachian orogen in Canada. *Can. J. Earth Sci.* **16**, 792-807.

________ & MALPAS, J. (1972): Sheeted dikes and brecciated dike rocks within transported igneous complexes, Bay of Islands, western Newfoundland. *Can. J. Earth Sci.* **9**, 1216-1229.

________ & SMYTH, W.R. (1973): Metamorphic aureoles beneath ophiolite suites and alpine peridotites: tectonic implications with west Newfoundland examples. *Am. J. Sci.* **273**, 594-621.

________ & STEVENS, R.K. (1974): The ancient continental margin of eastern North America. *In* The Geology of Continental Margins (C.A. Burk & C.L. Drake, eds.). Springer-Verlag, New York, N.Y. (781-796).

WILSHIRE, H.G. (1984): Mantle metasomatism: the REE story. *Geology* **12**, 395-398.

________ (1987): A model of mantle metasomatism. *In* Mantle Metasomatism and Alkaline Volcanism (E.M. Morris & J.D. Pasteris, eds.). *Geol. Soc. Am., Spec. Pap.* **215**, 47-60.

________, PIKE, J.E.N., MEYER, C.E. & SCHWARZMAN, E.C. (1980): Amphibole-rich veins in lherzolite xenoliths, Dish Hill and Deadman Lake, California. *Am. J. Sci.* **280**-A, 576-593.

Received November 12, 1995, revised manuscript accepted April 5, 1997.